CARBON CAPTURE THROUGH THE PROCESS OF ADSORPTION USING AGRICULTURAL WASTES AS THE ADSORBENT (CORN COBS)

BY

OSHIONIBU JEFFREY

ENG2002072

DEPARTMENT OF CHEMICAL ENGINEERING

FACULTY OF ENGINEERING

UNIVERSITY OF BENIN

EDO STATE, NIGERIA

OCTOBER, 2025

CARBON CAPTURE THROUGH THE PROCESS OF ADSORPTION USING AGRICULTURAL WASTES AS THE ADSORBENT (CORN COBS)

BY

OSHIONIBU JEFFREY

ENG2002072

A PROJECT SUBMITTED TO THE DEPARTMENT OF CHEMICAL ENGINEERING, UNIVERSITY OF BENIN, BENIN CITY, NIGERIA

IN PARTIAL FULFILLMENT OF THE REQUIREMENTS FOT THE AWARD OF BACHELOR OF ENGINEERING IN CHEMICAL ENGINEERING

OCTOBER, 2025

CERTIFICATION

This is to certify that this research project was carried out by OSHIONIBU JEFFREY with matriculation number ENG2002072 in the Department of Chemical Engineering, University of

Benin, Benin City, Edo State Nigeria.

Engr. Mrs. Edokpayi (Project Supervisor)	**Date**
Engr. Prof. S. E. Uwadiae (Project Coordinator)	**Date**
Engr. Prof. E. A. Oyedoh (Head of Department)	**Date**
External Supervisor	**Date**

DEDICATION

This project is dedicated to Almighty God for the strength, wisdom, and grace bestowed upon me throughout this journey.

I also dedicate this Project to my Mom, Mrs. Mike Cordelia, to my sisters, Judith and Jennifer Oshionibu, to my amazing friends Godson, Wisdom, Emmanuel, Henry, Dave, Godswill, Christabel, Trade Minded, and to my mentors, Engr. Mrs. Edokpayi and Dr. Fred.

ACKNOWLEDGEMENTS

I express my deepest gratitude to God almighty for the power and courage to complete this Project. My sincere gratitude goes to my Project Supervisor, Engr. Mrs. Edokpayi, for her constant support, patience and feedback throughout this research. I am also very grateful to my Mom, Mrs. Mike Cordelia for her constant love, financial support, and prayers.

I would also like to extend my sincere thanks to the Head of Department, Engr. Prof. E. A. Oyedoh. I am grateful for his/her/their leadership and for fostering a conducive academic environment in the Department of Chemical Engineering that encourages students to excel.

Lastly, I want to thank my friends, Godson (Big Jiggy), and the entire ENG70's for their encouragement and support.

ABSTRACT

Climate change driven by increasing atmospheric CO_2 concentrations calls for urgent implementation of atmospheric CO_2 reduction. However, adsorbents are mostly expensive and energy-intensive, especially for developing nations. Agricultural wastes, especially corn cobs, are a sustainable alternative due to their lignocellulosic composition, natural porosity, and abundance as underutilized biomass. This study investigated the CO_2 adsorption potential of chemically activated corn cob-derived adsorbent through packed bed column experiments.

Corn cobs were collected, processed, and activated using potassium hydroxide (KOH) at temperatures between 400-600°C. CO_2 gas was generated in-situ via $CaCO_3$-HCl reaction and passed through glass columns (2.1 cm diameter, 5 cm bed height) at flow rates of 0.5-2.0 L/min. Four particle size ranges (100, 250, 500, and above 500 μm) were evaluated over 60-minute contact periods at ambient temperature (29±2°C).

Characterization via SEM-EDS revealed highly porous morphology with 90.05% carbon content and oxygen-containing functional groups favorable for CO_2 binding. The 100 μm particle size achieved the highest equilibrium adsorption capacity of 5,459 ppm·L/g, while 250 μm particles demonstrated optimal removal efficiency of 48.0%. Breakthrough analysis indicated that smaller particles delayed saturation, with 100 μm maintaining effectiveness beyond 45 minutes compared to 25 minutes for above 500 μm particles. Flow rate influenced performance, with reduced rates (0.5 L/min) compensating for larger particle sizes by increasing contact time. These findings reveal that corn bobs are a viable solution for carbon capture.

TABLE OF CONTENTS

LIST OF FIGURES

LIST OF TABLES

NOMENCLATURE

CCS: Carbon Capture and Storage

CCUS: Carbon Capture, Utilization, and Storage

CFCs: Chlorofluorocarbons

DTG: Derivative Thermogravimetry

EDS: Energy Dispersive X-ray Spectroscopy

EOR: Enhanced Oil Recovery

FAOSTAT: Food and Agriculture Organization Statistical Database

HCFCs: Hydrochlorofluorocarbons

HFCs: Hydrofluorocarbons

IEA: International Energy Agency

IGCC: Integrated Gasification Combined Cycle

NASA: National Aeronautics and Space Administration

Ppm: Parts Per Million

PSA: Pressure Swing Adsorption

SEM: Scanning Electron Microscopy

SSA: Sub-Saharan Africa

TGA: Thermogravimetric Analysis

UN: United Nations

CHAPTER ONE

INTRODUCTION

1.1 Background of Study

Climate change is a major global crisis that has caused significant damage to the environment in recent years. Earth is currently facing rising average temperatures, shrinking ice caps, more frequent and severe weather events, and unpredictable climate changes (Yoro & Daramola, 2020). These changes have been linked to human activities, which release excessive amounts of greenhouse gases, particularly carbon dioxide (CO_2), into the atmosphere. According to the United Nations, human actions since the 1800s have played a significant role in altering the climate, leading to a temperature increase of approximately 1.1 °C compared to pre-industrial times (United Nations, 2022). Data from the National Aeronautics and Space Administration (NASA) shows a dramatic rise in global surface temperatures over the past two decades (NASAClimate, 2022). This can be attributed to the result of harmful practices meant to meet the growing global demand for energy. These practices are influenced by rapid population growth, industrial expansion, and changing lifestyles (Shirzad et al., 2019). Over the last several decades, global energy consumption has increased, with fossil fuels such as oil, gas, and coal being the main sources (OurWorldinData, 2022). Fossil fuel-based energy systems are responsible for releasing large quantities of greenhouse gases into the atmosphere (Ahmed et al., 2021). The main greenhouse gases responsible for global warming include carbon dioxide, methane, nitrous oxide, chlorofluorocarbons (CFCs), hydrochlorofluorocarbons (HCFCs), and hydrofluorocarbons (HFCs) (IEA, 2022). All available evidence points to a continuous and significant rise in CO_2 emissions, indicating a need for effective strategies to reduce greenhouse gas output and work toward a net-zero emissions future (Osman et al., 2022).

Carbon Capture, Utilization, and Storage (CCUS) technologies are one of the strategies used to reduce greenhouse gas output, curb carbon dioxide emissions and address climate change. These systems work by capturing CO_2 directly from major emission sources, such as fossil fuel power plants, cement factories, and other industrial processes, before the gas can escape into the atmosphere (Yaashikaa et al., 2023). Once captured, the CO_2 can be either permanently stored underground in deep geological formations or reused in various ways, including in the manufacturing of chemicals, synthetic fuels, and for enhanced oil recovery. Advancements in CCUS are making the technology more efficient and accessible. Innovations in adsorbent materials, selective membranes, and electrochemical methods have greatly increased capture performance while also helping to lower operational costs (Ketabchi et al., 2023; Soo et al., 2024). This progress makes CCUS a more attractive solution for industries under pressure to decarbonize.

One of the methods that can be used during the capture carbon is known as adsorption. Adsorption is a widely used method for removing pollutants from air and water. It works by using solid materials, known as adsorbents, to attract and hold unwanted substances, called adsorbates, on their surface (Abd et al., 2020). Depending on how the adsorbent interacts with the pollutant, adsorption can happen in two ways. If the attraction is weak, such as through natural surface forces, the process is called physical adsorption (Atif et al., 2022). On the other hand, when a stronger, more permanent bond forms between the adsorbent and the pollutant, it is referred to as chemical adsorption (Firdaus et al., 2021). In the case of carbon dioxide removal, the gas molecules stick to the surface of the adsorbent (Ben-Mansour et al., 2016). Many materials have been tested for their ability to capture CO_2, including organic and inorganic substances (Derylo-Marczewska et al., 2017). For example, amine-based compounds, metal oxides, and certain chemical materials have shown some success in

chemically binding with CO_2 (Song et al., 2020). These materials usually have special surface groups that help attract the gas (Balou et al., 2020).

Although traditional adsorbents often have strong adsorption abilities, they are not always feasible for large-scale carbon capture due to their high production costs. In contrast, agricultural waste provides a more affordable, renewable, and sustainable alternative as a raw material for adsorbent development (Othmani et al., 2022). These wastes are the solid by-products generated from crop and livestock activities. A major component of agricultural waste is lignocellulosic biomass, which is made up of complex plant-based substances such as cellulose, hemicellulose, lignin, pectin, as well as proteins, starches, and sugars. Agro-waste materials like bagasse, herbal residues, and corn straw have been widely studied as low-cost and renewable sources for producing activated carbon. Among these, corn cobs stand out not only because they are easily available, but also because of their composition, rich in cellulose (27.71%), hemicellulose (38.78%), and lignin (9.4%), and their naturally porous structure, which makes them promising for adsorption applications (Raghavendra et al., 2025). Based on the potential of this agricultural waste, this study focuses on the capture of carbon dioxide through adsorption, contributing to both environmental protection and waste management.

1.2 Statement of the Problem

While various carbon capture systems have been developed, many of them are still costly, technically sophisticated, or energy-intensive, making large-scale implementation challenging, particularly in developing countries. At the same time, massive amounts of agricultural waste, such as corn cobs, are produced and frequently thrown or underutilized, raising both environmental and economic concerns. Although a few studies has looked into low-cost adsorbents, there is currently a scarcity of studies on the carbon capture potential of

commonly available agricultural waste. This study aims to assess the effectiveness of corn cobs as natural adsorbents for CO_2 removal.

1.3 Aim and Objectives

The aim of this study is to investigate the potential of agricultural wastes, specifically corn cobs, as low-cost, sustainable adsorbents for the capture of carbon dioxide (CO_2) through the process of adsorption. The specific objectives of this study includes:

1. To characterize the physical and chemical properties of corn cobs relevant to adsorption.
2. To experimentally test the CO_2 adsorption capacity of corn cobs
3. To compare the performance of the adsorbent in capturing CO_2.
4. To evaluate the cost-effectiveness and sustainability of using corn cobs for carbon capture.

1.4 Scope of the Study

This study evaluates the CO_2 adsorption potential of one commonly available agricultural waste: corn cobs. The research include gathering, processing, and perhaps altering these materials for use as adsorbents. Laboratory studies will be conducted to determine their effectiveness in capturing CO_2, with data analysed to compare adsorption capabilities. The study focusses on these two waste kinds and seeks to determine their potential as low-cost, ecologically friendly alternatives to traditional carbon capture materials.

1.5 Relevance of the Study

Carbon capture methods must be affordable and effective to address the global climate crisis caused by rising CO_2 emissions. Traditional technologies are frequently expensive and resource-intensive, limiting their application in many areas. This study provides a sustainable

alternative by utilising agricultural wastes, which are inexpensive, readily available, and underutilised. Repurposing these materials is a cost-effective way to capture CO_2 and addresses the growing issue of agricultural waste disposal. Scientifically, the study fills a research gap by evaluating the adsorption capability of these specific waste materials, providing valuable data for future studies in carbon capture and environmental management.

CHAPTER TWO

LITERATURE REVIEW

2.1 Agricultural Waste

2.1.1 Corn and Corn Cobs

Corn or maize (*Zea mays* L.) is an important annual cereal crop of the world belonging to family Poaceae. Zea is an ancient Greek word which means “sustaining life” and Mays is a word from Taino language meaning “life giver.” The word “maize” is from the Spanish connotation “maiz” which is the best way of describing the plant. Various other synonyms like zea, silk maize, makka, barajovar, etc. are used to recognize the plant (Kumar & Jhariya, 2013). It is considered as a staple food in many parts of the world. It is a third leading crop of the world after rice and wheat (Sandhu, Singh, & Malhi, 2007). Its taxonomy is presented below:

Kingdom: Plantae

Subkingdom: Tracheobionta

Superdivision: Spermatophyta

Division: Magnoliophyta

Class: Liliopsida

Subclass: Commelinidae

Order: Cyperales

Family: Poaceae

Subfamily: Panicoideae

Tribe: Andropogoneae

Genus: *Zea*

Species: *Zea mays*

As in other countries of SSA, maize is an important crop in Nigeria, where it is cultivated by smallholder farmers over 6.5 million hectares of land across diverse agroecological zones of the country (Onumah et al., 2021; pwc, 2021; FAOSTAT, 2022). It is by far the largest cereal crop in terms of area and production volume and is the most consumed staple food in Nigeria (Onumah et al., 2021). In Nigeria, maize is widely used for human consumption, in animal feed, pharmaceutical industries, food manufacturers, breweries, flour mills and other industries. Nearly 80 percent of the maize grain is used for human consumption and animal feed with the remaining 20 percent utilized for industrial processing of diverse products (Onumah et al., 2021). With a per capita consumption of about 35 kg per person per year, maize accounts for an estimated 10% of the daily calorie intakes in the country. The crop is also an important source of cash income for farmers and contributes significantly to agro-industrial development particularly in the livestock feed industry (Alene et al., 2009; Wossen et al., 2017b).

Following its arrival in West Africa in the 15th century (Miracle, 1965), maize became an invaluable crop fitting into the existing diverse farming systems because of its broad adaptation to varying growing conditions, ease of processing and resistance to pre-harvest bird damage that plagued sorghum, millet, and rice (McCann, 2005; Fakorede et al., 2022). As a quick maturing crop, it has become a critical source of food for rural families when food reserves are depleted before the root crops, sorghum, millet, and other native crops are harvested. Until the 1970s, maize was mainly grown in the humid forest agro-ecology as a source of fresh maize for boiling and roasting, and grain for processing and conversion into diverse local food products (Fajemisin, 2014). It is now cultivated even in the drier areas which are traditional niches for sorghum and millet due to the development and commercialization of drought tolerant extra-early and early maturing maize varieties that provide food when grain reserves are depleted after the long dry period because of their faster

maturity cycle and better responsiveness to fertilizer compared to sorghum and millet (Badu-Apraku et al., 2015; Fajemisin, 2014).

2.1.1.1 Chemical Composition Corn Cobs

Several studies have reported that corn cobs are primarily composed of lignocellulosic materials, with an estimated range of 33–43% cellulose, 26–36% hemicellulose, and 17–21% lignin (Bhatia et al., 2020). Among these, hemicellulose content is notably higher compared to other biomass sources, making corn cobs a valuable feedstock for the commercial production of compounds such as xylitol and furfural due to their high xylan levels (Hoang et al., 2020). Sugars extracted from corn cobs have also been utilized in the microbial synthesis of various acids, including propionic, levulinic, lactic, acetic, butyric, and malic acids, and in the production of alcohols like ethanol, butanol, and 2,3-butanediol (Liu et al., 2012; Wang et al., 2019; Guo et al., 2010; Zheng et al., 2018; Zou et al., 2015). Additionally, pretreated corn cobs have served as carbon sources in solid-state and submerged fermentations, as well as in the generation of biofuels like biogas and bio-hydrogen. They have also been explored as low-cost biosorbents for removing heavy metals, dyes, and ions from wastewater (Gandam et al., 2022). According to Kaliyan and Morey (2010), corn cobs contain approximately 41.4% hemicellulose, 40% cellulose, and 5.8% lignin, along with small amounts of protein (2.5%), starch (2.1%), ash (1.8%), water-soluble carbohydrates (1.1%), and fat (0.7%). Lau (2018) adds that more than 60% of sweet corn cobs consist of insoluble dietary fibre, with cellulose being predominant, followed by hemicelluloses. Elemental analysis by Mullen et al. (2010) revealed the presence of elements such as silicon (5.33 g/kg), potassium (10.8 g/kg), phosphorus (1.11 g/kg), magnesium (0.55 g/kg), calcium (0.23 g/kg), sulfur (0.14 g/kg), and trace levels of aluminium, barium, and strontium. Furthermore, corn cobs have demonstrated antioxidant properties, which are linked to their phenolic content (Lau, 2018).

2.1.1.2 Uses of Corn Cobs in Adsorption Studies

Corn cobs, as a lignocellulosic biomass, have gained considerable attention as a sustainable, low-cost, and effective adsorbent material in environmental remediation. Several studies have demonstrated their applicability in adsorbing pollutants from wastewater and gases, owing to their high cellulose and hemicellulose content, large surface area after activation, and abundance as agricultural waste.

In a fixed-bed column study, Igwegbe et al. (2021) evaluated activated carbon derived from corn cobs (CCAC) for removing oil and grease from refinery wastewater. The research showed that corn cob-based adsorbents performed effectively, with removal efficiencies ranging from 15% to over 60%, depending on key variables like particle size, feed concentration, and bed height. Smaller particle sizes and taller adsorption beds improved performance, as they increased the contact time and surface area for adsorption. Additionally, modeling using Bohart–Adams kinetics accurately predicted the breakthrough behavior, indicating reliable performance and suitability for industrial scale-up. The findings confirmed that corn cobs, after chemical activation, exhibit favorable adsorptive characteristics and practical application potential in treating oily industrial effluents.

Gotore et al. (2020) showed that activated carbon derived from maize cobs (MCAC) achieved high removal efficiency for nickel ions, emphasizing the role of contact time and adsorbent dosage as critical parameters influencing adsorption performance. Their findings align with the broader consensus that corn cobs possess favorable properties, such as high surface area, porosity, and reactivity, that make them suitable for adsorption applications in water treatment. These results support the growing recognition of agricultural waste materials as viable alternatives to conventional adsorbents, particularly for toxic metal removal.

Thuy and Khu (2022) investigated the preparation and application of corn cob-derived activated carbon for carbon dioxide (CO_2) adsorption. The activated carbon was produced using a chemical activation process with potassium hydroxide (KOH) as the activating agent. The activation conditions were rigorously controlled, involving carbonization of the corn cob biomass at 450°C under a nitrogen atmosphere, followed by KOH impregnation and high-temperature activation at different temperatures (700–850°C). Importantly, the study emphasized that the adsorption efficiency was not solely dependent on the surface area but was also significantly enhanced by the presence of carboxylic groups, which provided active sites for CO_2 binding. The findings clearly demonstrated that corn cob waste can be effectively valorized into a high-performance adsorbent for environmental applications such as greenhouse gas capture. It also positioned corn cobs as a low-cost, sustainable, and renewable raw material for developing carbon-based adsorbents with competitive efficiency.

The application of corn cobs in adsorption studies has shown significant promise, especially in the development of activated carbon for removing harmful substances from the environment. Collectively, these studies demonstrate that when properly processed, corn cobs can serve as efficient, low-cost adsorbents with high surface area and functional group content. This not only adds value to agricultural waste but also contributes to sustainable environmental management through effective pollutant capture, such as carbon dioxide, highlighting corn cob's viability in advanced adsorption technologies.

2.2 Carbon Capture

Over the past several decades, increasing atmospheric CO_2 concentrations, mostly attributed to anthropogenic activities like fossil fuel combustion, have intensified the greenhouse effect, presenting substantial risks to human and environmental security. Currently, the atmospheric CO_2 level has surpassed 400 ppm, which represents a roughly 40% increase compared to pre-

industrial levels. This rise has contributed to a global temperature increase of approximately 0.8°C (Leung et al., 2014). Although renewable energy sources are gaining traction, transitioning entirely from traditional fossil-based power systems remains impractical in the near future. The International Energy Agency has highlighted that while global carbon emissions temporarily decreased due to the COVID-19 pandemic, they are expected to rebound as global economic activities resume, showing no clear evidence of having reached peak emission levels.

To meet the global temperature containment target of 2°C, urgent action is required to overhaul current energy systems. In addition to accelerating the deployment of renewable energy, Carbon Capture, Utilization, and Storage (CCUS) technologies have garnered significant academic and industrial interest. These technologies offer a promising approach to reducing carbon emissions at scale and are recognized as a crucial component of global climate change mitigation efforts. CCUS involves the targeted removal of carbon dioxide from industrial emission streams, such as those from power plants, steel, and cement facilities, followed by its transport through pipelines for either permanent storage or beneficial reuse.

The CCUS process encompasses four core phases: capturing carbon dioxide from emission sources, transporting it, utilizing it in various industrial applications, and storing it securely (Müller et al., 2020). Its development dates back to the 1970s, with the first large-scale implementation recorded in 1972 at the Kelly Snyder oil field in Texas, USA (Orujov et al., 2023). Initially focused on enhanced oil recovery (EOR) and natural gas purification, CCUS technologies have evolved to address broader environmental objectives. Projects like the Enid fertilizer plant in Oklahoma and Norway's Sleipner gas field project have demonstrated the feasibility of long-term CO_2 sequestration, capturing hundreds of thousands to millions of tons annually.

While originally used to purify industrial gases, CCUS technologies are now increasingly integrated into sectors like coal gasification and petroleum refining. High-profile implementations include the Great Plains Coal Gasification project in the U.S. and Canada's Weyburn-Midale initiative. These projects highlight the strategic shift toward storing CO_2 in deep geological formations to reduce atmospheric concentrations. Notably, in 2014, SaskPower in Canada pioneered the world's first commercial-scale CO_2 capture project for a coal power plant, achieving daily capture rates up to 2852 tons. Innovative efforts such as Sweden's Hybyrit project, which seeks to replace traditional coke in ironmaking with hydrogen produced from renewable electricity, aim to achieve near-zero emissions.

Despite progress, CCUS remains in a developmental stage due to its high implementation costs, especially during the capture phase, which accounts for 60–70% of total system expenses (Dubey & Arora, 2022). These costs include energy requirements, chemical inputs, and equipment investment. For concentrated CO_2 streams, like those from ethanol or natural gas plants, capture costs range from $15 to $25 per ton. However, for dilute sources such as cement and power plants, costs can escalate to $40–120 per ton (Baylin-Stern & Berghout, 2021). Transporting captured CO_2 incurs additional infrastructure and operational costs, while storage requires investment in suitable geological reservoirs.

According to the International Energy Agency's CCUS roadmap, efforts are underway to make these technologies commercially viable by 2050 through integrated demonstration projects and cost reduction strategies (IEA, 2013). As such, the economic burden of CO_2 capture remains the most significant barrier to widespread adoption, but continued innovation and policy support may accelerate its global implementation (Liu et al., 2022a; Storrs et al., 2023)..

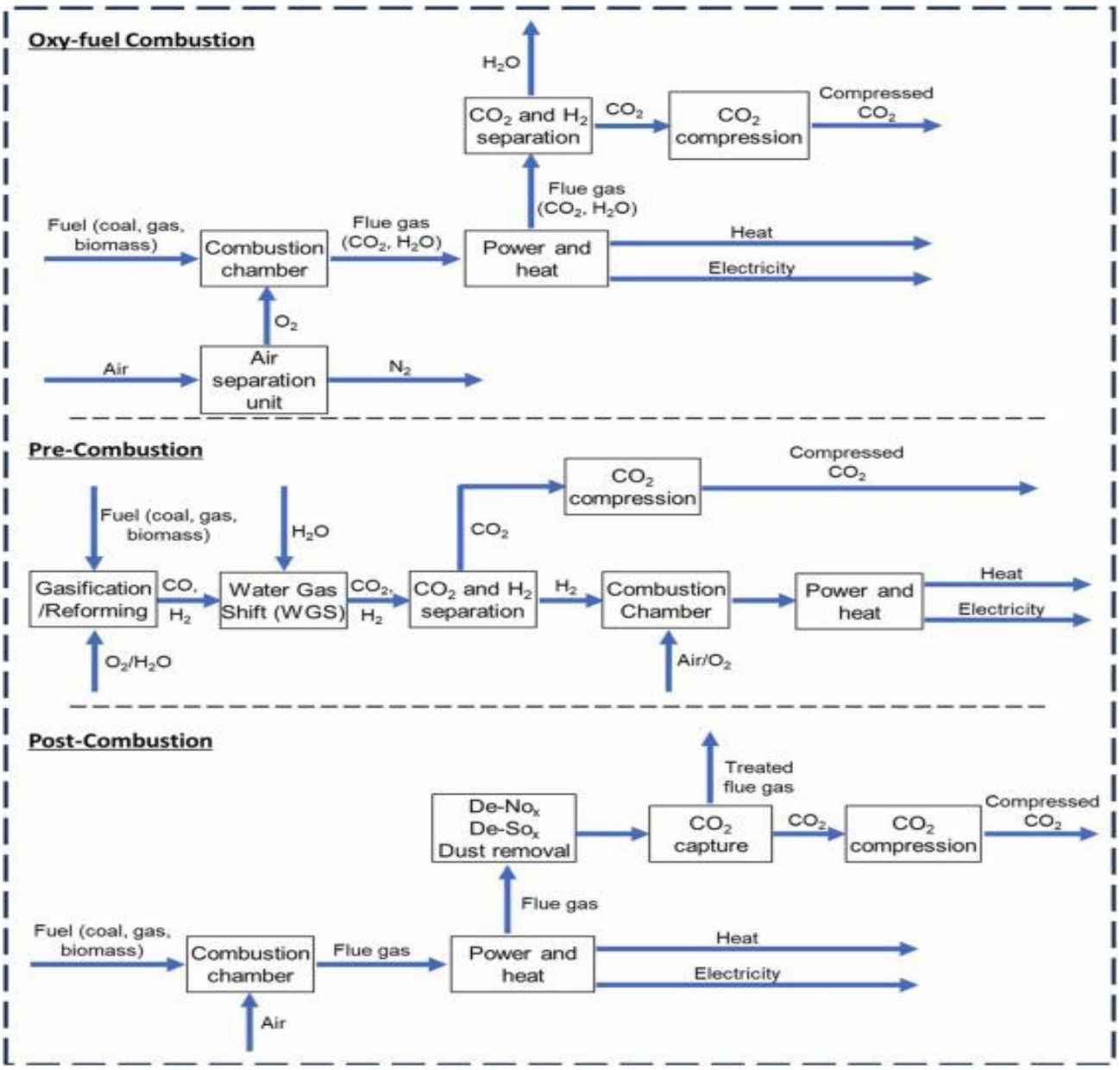

2.2.1 Types of Carbon Capture Technologies

Figure 2.1 Process of Carbon Capture Technologies (Soo et al. 2024)

2.2.1.1 Pre-Combustion Carbon Capture

Pre-combustion carbon capture involves converting fuel, such as coal, natural gas, or biomass, into a gas mixture made up of carbon monoxide (CO) and hydrogen (H_2) through a reforming or gasification process. This is followed by a water–gas shift reaction, where CO reacts with

steam to form CO_2 and more hydrogen. The resulting gases are then separated to extract the CO_2 for capture and storage or use. This approach is commonly used in systems like Integrated Gasification Combined Cycle (IGCC) plants. In IGCC, steam and oxygen are introduced into a gasifier to produce syngas, a mixture of CO and H_2. The syngas is cleaned of ash in a cyclone separator and then passed through a water–gas shift reactor to convert more CO into CO_2. Before CO_2 can be captured, the gas undergoes desulfurization to remove sulfur compounds. After that, the CO_2 is separated and either stored or reused, while the remaining hydrogen is used to fuel a gas turbine (Theo et al., 2016). Pre-combustion capture is highly efficient, primarily because it deals with CO_2 before combustion, when it is more concentrated. However, the process can be quite costly due to the complex equipment required, especially the gasifier. To extract CO_2, both chemical and physical absorbents are used. Chemical methods involve materials like carbonates, while physical methods use solvents like methanol or polypropylene glycol. These methods are widely adopted in industrial applications. Although pre-combustion systems can achieve over 90% CO_2 removal, they often lead to a drop in overall plant efficiency due to the high energy demand (Olabi et al., 2022). An alternative and more cost-effective method under pre-combustion capture is the Calcium Looping (CaL) process. In this technique, calcium oxide (CaO) binds with CO_2 to form calcium carbonate ($CaCO_3$), which is then heated to release pure CO_2. This process can be repeated several times, and waste heat from the system can be reused, helping to lower energy costs while maintaining high capture efficiency (Wu et al., 2019). A practical example of pre-combustion carbon capture is seen at the Port Arthur demonstration plant in the United States, which has successfully captured over 1 million tons of CO_2. The plant utilizes a dual pressure swing adsorption (PSA) system. When gas pressure is low, hydrogen is purified and the remaining gas undergoes vacuum PSA to recover CO_2. When the gas is under high pressure, CO_2 is extracted directly, and hydrogen is purified from the remaining stream. This

setup proves that high-purity hydrogen (over 99.9%) and efficient CO_2 capture can be achieved simultaneously (Grande et al., 2017).

2.2.1.2 Post-Combustion Carbon Capture

Post-combustion carbon capture focuses on extracting CO_2 from flue gases emitted after the combustion of fuels. These flue gases are typically made up of nitrogen and carbon dioxide at elevated temperatures (120–180 °C), along with traces of steam, sulfur dioxide, nitrogen oxides, and fine particulate matter like fly ash (Council, 2011). In compliance with environmental standards (Ma et al., 2015), harmful gases in the flue stream are removed before release into the atmosphere. Since carbon dioxide exists at relatively low concentrations (typically between 3–20%) in post-combustion gases, much lower than in pre-combustion processes, more selective and efficient capture techniques are required (Li et al., 2019). Chemical absorption, particularly using aqueous monoethanolamine (MEA), is the most common technique. MEA reacts with CO_2 to form carbamate compounds, making it highly effective for this application (Wilberforce et al., 2019). The capture process involves two main stages: first, the flue gas passes through an absorber where the MEA captures CO_2. Then, the CO_2-rich solvent is directed to a regeneration unit where heat is applied to release pure CO_2. The regenerated MEA is cycled back for reuse, and the captured CO_2 is compressed and prepared for storage or utilization (Kanniche et al., 2010). Post-combustion capture stands out for its adaptability. It can be retrofitted into existing fossil-fuel-based power plants without needing to overhaul the infrastructure, unlike pre-combustion systems (Li et al., 2019). However, this advantage comes with a trade-off: high energy demands**.** A substantial amount of energy is required for solvent regeneration and CO_2 compression. For example, a typical coal-fired plant capturing around 800 tonnes of CO_2 per day might face an

increase in electricity generation costs of up to 65% due to these additional energy needs (Wu et al., 2018).

2.2.1.3 Oxy-Combustion Carbon Capture

Oxy-fuel combustion is another effective pathway for carbon capture, operating distinctly from pre-combustion methods. In this approach, fuel is burned using pure oxygen instead of atmospheric air, with oxygen primarily produced through cryogenic air separation or, less commonly, through water electrolysis (Stanger et al., 2015). After the combustion process, which also involves soot removal, a portion of the flue gas which is rich in CO_2 is recycled back into the combustion chamber. This gas recycling helps regulate the combustion temperature while also increasing the CO_2 concentration in the flue gas, making downstream separation more straightforward (Osman et al., 2021). Initially introduced in the 1980s, oxy-fuel combustion aimed to generate flue gas streams with high CO_2 purity, around 95% after the removal of water vapor (Richter and Chen, 1989), There are two primary applications of this method in power generation: pulverized coal-fired oxy-fuel combustion (oxy-PC) and circulating fluidized bed systems (oxy-CFBs) (Yang et al., 2020). In the oxy-PC approach, pulverized coal is combusted in specially designed boilers, a process well-documented in the literature (Toftegaard et al., 2010). The oxy-CFB process, by contrast, employs a different boiler design and introduces limestone during combustion, which aids in in-situ sulfur capture (Go et al., 2023). A significant environmental advantage of oxy-fuel combustion lies in its reduction of nitrogen oxide (NO_x) emissions. This benefit arises due to the suppression of thermal NO_x formation, which is made possible through better flame temperature control and the recycling of NO_x-laden flue gases, which promotes their decomposition upon re-entry into the combustion zone (Ndibe et al., 2013). However, in the case of oxy-CFB systems, the inclusion of limestone may offset this advantage, as it can increase NO_x emissions depending

on the operating temperature (Yang et al., 2020). While oxy-fuel combustion holds strong technical merit, it is also associated with considerable economic and efficiency challenges. The need for oxygen generation, primarily through air separation, adds substantial capital and energy costs. Despite this, techno-economic evaluations show that oxy-fuel combustion, when implemented with heat-integration strategies in coal-fired plants, can limit the cost of CO_2 avoidance to around USD 43.24 per ton (Yuan et al., 2024). Nevertheless, one of the biggest technical drawbacks is a decline in net plant efficiency, which can reach a reduction of 10.41%, mostly due to the high energy input required for oxygen production and flue gas handling (Yuan et al., 2024). Applications of oxy-fuel combustion beyond traditional power plants are also under active exploration. For example, its use on marine vessels has been analyzed as a pathway for onboard CO_2 capture (Wohlthan et al., 2024). However, the need for onboard oxygen production presents serious constraints, such as elevated energy consumption and diminished engine performance. An alternative proposal suggests supplying liquefied oxygen from port facilities, thereby eliminating the need for onboard oxygen generation. This adjustment would enhance overall efficiency but would necessitate larger oxygen storage systems onboard (Wohlthan et al., 2024).

2.2.2 Challenges and Opportunities of Carbon Capture Technologies in Nigeria

Implementing Carbon Capture and Storage (CCS) technology in Nigeria is limited by various challenges including technical, financial, regulatory, and socio-political dimensions. These barriers significantly limit Nigeria's ability to apply CCS as a climate mitigation tool, despite its promising benefits. From a technical perspective, the most pressing challenge is the absence of dedicated infrastructure to support the full CCS chain, from CO_2 capture to its eventual transport and storage. Much of Nigeria's existing infrastructure is oriented around the oil and gas sector and is ill-suited to accommodate CCS operations (Dike & Akani, 2020).

Beyond infrastructure, there is a serious shortage in local technical expertise. The engineering knowledge and operational experience required to design and maintain CCS systems are scarce in Nigeria, making it difficult to initiate or scale such projects (Betiku & Bassey, 2022). Bridging this gap would require deliberate investments in capacity-building efforts, including specialized training and curriculum development in higher education institutions. Additionally, Nigeria's research and development landscape is still evolving when it comes to CCS. Although there has been some exploratory studies conducted on geological storage options (Yahaya-Shiru et al., 2023; Ojo & Tse, 2016), there is a lack of comprehensive R&D that spans the entire value chain, capture, transport, utilization, and storage.

Economic and financial challenges further complicate CCS deployment in Nigeria. The technology itself involves huge capital and operating costs, particularly in the areas of CO_2 capture and long-distance transport. These costs, in a developing economy like Nigeria, where budgetary allocations are often stretched across many urgent socio-economic needs, they become burdensome (Dioha et al., 2019). Limited funding, both from public and private investors, has made financing CCS projects extremely difficult. The high-risk nature of CCS investments, coupled with uncertain long-term returns, deters private sector participation (Betiku & Bassey, 2022). Moreover, in the absence of a functioning carbon pricing mechanism or policy-driven incentives, CCS projects struggle to demonstrate economic viability. The cost of capturing emissions from industries or power stations often outweighs the benefits when there is no clear financial gain for emission reductions (Mohammed, 2020).

Nigeria also lacks a comprehensive and unified legal framework to support CCS deployment. Current environmental and energy regulations are fragmented and do not properly address the complexities of CCS operations across capture, transport, and storage phases (Dike & Akani, 2020). This contributes to investor hesitation and operational risks. The absence of policies

that define responsibilities, environmental safety, and liability further weakens the environment. For CCS to take root in Nigeria, government intervention is critical. Well-defined policies and regulatory reforms are needed (Onwuka & Adu, 2024). Learning from countries with more advanced CCS policies, such as the United Kingdom, could help Nigeria adopt the procedure properly (Betiku & Bassey, 2022).

Despite these challenges , there are several opportunities CCS presents for Nigeria. Nigeria is richly endowed with geological formations that are suitable for long-term carbon dioxide storage. Among the most promising areas is the Niger Delta, home to numerous hydrocarbon fields that can be reused for carbon storage. For example, research conducted by Ojo and Tse (2016) identified sandstone reservoirs in the Coastal Swamp depobelt as having the right characteristics for secure CO_2 storage such as adequate depth, porosity, permeability, and a thick caprock layer. Their assessment estimates that these formations could accommodate up to 147 million tons of CO_2, making them valuable assets. Also, Yahaya-Shiru et al. (2023) carried out a geomodeling analysis on the 'X-Field' in the Central Swamp II depobelt, concluding that the site holds an estimated cumulative storage potential of 7.01 billion standard cubic meters. These studies confirm that Nigeria's geology not only supports safe and permanent CO_2 storage but can also take advantage of its existing oil and gas infrastructure to accelerate CCS project development.

CCS also offers significant economic advantages that can catalyze sustainable development in Nigeria. One major benefit is the potential for job creation across various segments of the CCS value chain, including CO_2 capture, transport, and storage infrastructure. This could be especially transformative for the country, as this may generate new livelihoods and economic activities for communities traditionally reliant on oil and gas (Dioha et al., 2019). In addition to employment, CCS can stimulate technological growth by encouraging the development

and deployment of advanced climate technologies. Through this, Nigeria can strengthen its industrial base and carry out innovations that encompass other sectors, such as renewable energy (Betiku & Bassey, 2022).

The primary environmental merit of CCS lies in its capacity to significantly reduce greenhouse gas emissions, thereby contributing to global climate mitigation efforts. CCS prevents large volumes of CO_2 from being released into the atmosphere by capturing carbon dioxide directly from industrial and power generation sources, helping to reduce Nigeria's overall carbon footprint (Bui et al., 2018). This is important for Nigeria, which continues to rely heavily on fossil fuels for electricity generation. With CCS, the country can maintain energy security (Dioha et al., 2019). By adopting this technology, the country can demonstrate commitment to emissions reduction without affecting economic progress.

2.3 Adsorption

Adsorption refers to the process where molecules from a gas or liquid adhere to the surface of a solid material, known as the adsorbent (Abin-Bazaine et al., 2022). This surface phenomenon is primarily influenced by intermolecular forces and is generally classified into two main types: physical adsorption (physisorption) and chemical adsorption (chemisorption). Physisorption is driven by weak van der Waals forces, making it a low-energy and reversible process. In contrast, chemisorption involves the formation of chemical bonds between the adsorbate and the adsorbent surface, resulting in a stronger, often irreversible, interaction (Huber et al., 2019).

In practical applications, adsorbents interact with contaminants through either of these mechanisms, and understanding the distinction between the two is essential when choosing an appropriate material for pollutant removal. Physisorption, due to its reliance on weak

forces, is commonly utilized by materials like activated carbon and nanocellulose. These adsorbents have high surface areas and porous structures, making them effective for removing organic pollutants, dyes, and volatile compounds from air or water.

Chemisorption, by contrast, involves stronger ionic or covalent bonds and is typically employed by advanced materials such as zeolites, modified clays, and metal–organic frameworks (MOFs). These adsorbents are particularly effective in capturing heavy metals and inorganic contaminants because they form stable chemical complexes with the target pollutants..

2.3.1 Factors Affecting Adsorption

The interaction between an adsorbent and the particles it captures, adsorbates, is significantly influenced by the intrinsic characteristics of the adsorbent. Factors such as molecular size, shape, polarity, radius, solubility, and the presence of functional groups all play a role in determining adsorption efficiency. When multiple substances are present in a solution, adsorption tends to be selective, with certain components binding preferentially to the surface. Adsorbents with higher molecular weights generally have greater adsorption potential, as they can anchor to the surface at multiple points. Additionally, the presence of aromatic rings in an adsorbent's structure enhances its ability to interact with various surfaces, thereby improving its efficiency (Nikolic & Agababa, 2009). The physical and chemical makeup of the adsorbent, especially its particle size and surface uniformity, also affects performance. Smaller particles increase the rate of adsorption by facilitating faster diffusion of adsorbates to the surface. Furthermore, the size and distribution of pores within the adsorbent are critical for enabling effective transport of pollutants to active sites (Aljamali, 2020). Solution pH is another important factor, as it alters the charge and activity of functional groups on both the adsorbent and adsorbate. This is particularly relevant in applications such as gas purification,

odor control, removal of heavy metals, and drug adsorption using materials like activated carbon or clay.

2.3.2 Carbon Capture through Adsorption

Absorption is one of the most commonly used techniques for capturing carbon dioxide from gas streams, particularly those produced by power generation and industrial operations. In this method, a liquid substance, referred to as the absorbent, selectively absorbs CO_2 from a gas mixture. This typically takes place in an absorption tower or column where the gas stream is brought into contact with the absorbent. As the gas passes through the tower, CO_2 molecules dissolve into the liquid absorbent, allowing other gases to pass through unaffected (Nwaoha et al., 2016). The CO_2-loaded solvent is then transferred to a regeneration unit where heat is applied to release the absorbed carbon dioxide (de Meyer & Jouenne, 2022). Once regenerated, the solvent can be reused in the cycle, while the extracted CO_2 is compressed for storage or applied in processes like enhanced oil recovery or the production of industrial chemicals.

There are two major approaches to this method: physical and chemical absorption (Ochedi et al., 2020). Chemical absorption relies on solvents that react chemically with CO_2, while physical absorption depends on Henry's law, where CO_2 solubility in a solvent increases with pressure. Physical absorption works best under high pressure and low temperature. In this case, CO_2 is dissolved into the bulk of the solvent and released either by reducing pressure, raising temperature, or both. However, physically absorbing CO_2 from flue gas, which typically has low CO_2 partial pressure, requires significant energy input to pressurize the gas stream.

In chemical absorption, CO_2 reacts with solvents, commonly amine or carbonate solutions, to form weakly bonded intermediates that release CO_2 upon heating (Shah et al., 2020). This

method is particularly efficient in conditions of lower CO_2 partial pressure and is widely used in carbon capture due to its selectivity and reusability.

Physical absorption systems are especially suitable for high-pressure gas streams, such as those in pre-combustion capture processes like Integrated Gasification Combined Cycle (IGCC) systems. In these setups, after CO_2 is absorbed, the remaining hydrogen-rich syngas is combusted to generate electricity. The solvent that has captured CO_2 is regenerated either by flash desorption, which involves lowering pressure in stages to release the gas, or by stripping, where an inert gas like nitrogen is used to remove any remaining CO_2 after initial degassing (Spigarelli & Kawatra, 2013).

This chapter has examined the major carbon capture technologies including pre-combustion, post-combustion, oxy-fuel combustion, and adsorption, with a focus on their working principles, strengths, limitations, and relevance to Nigeria's context. Among these, adsorption has emerged as a valuable technique due to its cost-effectiveness, simplicity, and potential for deployment using locally available biomass-based adsorbents such as corn cobs. It was also established that although Nigeria possesses the geological capacity for long-term CO_2 storage, certain barriers continue to limit CCS deployment. This study seeks to contribute to available literature by investigating the adsorption efficiency of corn cobs for CO_2 capture.

CHAPTER THREE

METHODOLOGY

3.1 Materials

3.1.1 Apparatus and Equipment

Crucibles: Used for heating samples at high temperatures during the carbonization process, especially in the muffle furnace.

Figure 3.1 Crucibles

Muffle furnace: Used for carbonizing the corn cob samples by subjecting them to high temperatures in an oxygen-limited environment.

Figure 3.2 Muffle furnace

Beakers and conical flasks: Used for mixing chemicals, holding solutions, and carrying out reactions.

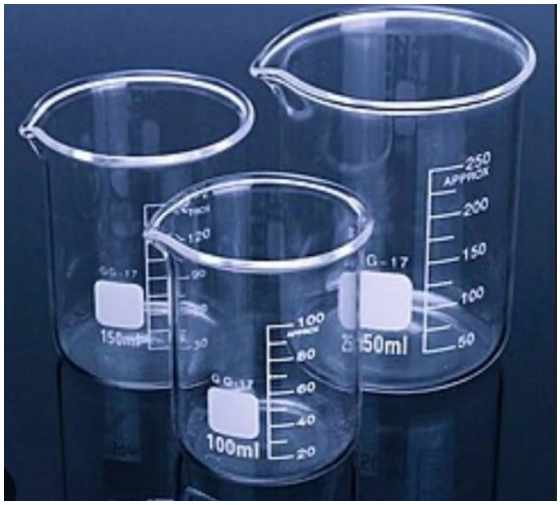

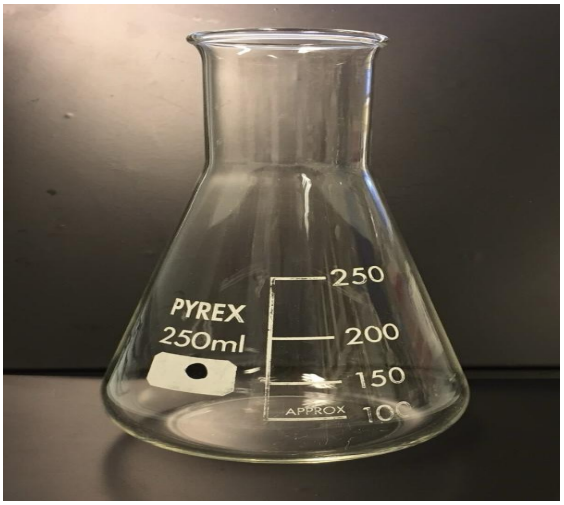

Figure 3.3 Beakers and concical flasks

CO_2 gas cylinder: Used to provide a continuous flow of carbon dioxide gas used for the adsorption experiments and for testing the CO_2 capture efficiency of the prepared adsorbents.

Figure 3.4 CO_2 gas cylinder

CO_2 detector: Used to monitor and measure the concentration of CO_2 in the setup before and after adsorption.

Figure 3.5 CO_2 detector

Desiccator: Used for cooling and preserving samples in a moisture-free environment after heating.

Figure 3.6 Desiccator

Mechanical grinder: Used to grind samples into fine powder.

Figure 3.7 Mechanical Grinder

pH meter / pH paper: Used to measure and monitor the pH of the adsorption medium.

Figure 3.8 pH meter

Stirring rod: Used for manually stirring solutions and suspensions during sample preparation.

Figure 3.9 Stirring rod

Oven: Used to remove moisture from corn cob samples before carbonization or activation.

Figure 3.10 Oven

Weighing balance: Used to accurately measure the mass of raw materials and adsorbents for

carbonization, activation, and adsorption experiments.

Figure 3.11 Weighing Balance

Sieve: Used to separate the adsorbent particles by size after grinding, ensuring uniform particle distribution and removing impurities.

Figure 3.12 Sieve

3.1.2 Materials, Reagents and Chemicals

1. Corn cobs
2. Potassium Hydroxide (KOH) Chemical activator)
3. CO_2
4. $CaCO_3$
5. $CaCl_2$
6. Distilled water
7. Dilute hydrochloric acid
8. Sodium hydroxide (NaOH) for pH adjustments

3.2 Methods

3.2.1 Collection and Preparation of Adsorbents

Corn cobs were obtained from New Benin and Oba Markets in Benin City, Nigeria. The material was first washed thoroughly with clean water to remove surface dirt and impurities, then rinsed with distilled water. It was air-dried for 24 hours and subsequently oven-dried at 105 °C for 4 hours to eliminate moisture. After drying, the corn cobs were crushed using a mechanical grinder and sieved to obtain uniform particle sizes suitable for activation. The

prepared corn cob powder was stored in an airtight container, and stored in an airtight container for activation.

3.2.2 Chemical Activation of Adsorbents

The activation process began by impregnating the biomass (corn cobs) in a potassium hydroxide (KOH) solution. A 1:1 weight ratio of KOH to dry biomass was used for the sample (14.029g KOH to 14.03g biomass). The mixture was stirred and allowed to soak at room temperature for 12 hours to ensure thorough penetration of the activating agent into the structure of the biomass. After soaking, the sample was filtered and dried again to remove excess moisture. The impregnated biomass was then subjected to carbonization in a muffle furnace under nitrogen atmosphere to prevent oxidation. The sample was heated at a controlled rate of 10 °C/min to target activation temperatures ranging between 400°C and 600°C, and held for 60–90 minutes depending on the sample. After carbonization, the resulting activated carbon was allowed to cool under nitrogen flow. The carbon was then washed with hot distilled water to remove residual acid and any soluble impurities, until the rinsing water reached neutral pH. Finally, the activated carbon was oven-dried at 110°C for 12 hours and stored in a desiccator for subsequent CO_2 adsorption experiments.

3.2.3 Preparation of Adsorbate (CO_2)

Two sources of carbon dioxide (CO_2) were used during the adsorption experiments. For the first two runs CO_2 was supplied from the exhaust of a portable generator, for the last two runs, the CO_2 was obtained from a cylinder containing the gas, purchased commercially. The variation in CO_2 source and flow rate resulted in observable differences in pressure across experiments. The cylinder-supplied CO_2 provided a steady and regulated flow, while the generator exhaust produced a lower and less stable pressure. All adsorption experiments were carried out under laboratory conditions.

3.2.4 Batch Adsorption Experiments

Batch adsorption experiments were conducted to evaluate the CO_2 adsorption behavior of activated carbon produced from corn cobs. The effects of contact time, adsorbent dosage, and initial CO_2 concentration were investigated under controlled conditions. Multiple impregnation ratios were tested (1:1, 2:1) to determine the optimal activating agent to biomass ratio for maximum CO_2 adsorption capacity. The adsorption experiments were conducted in a glass column with an internal diameter of 2.1 cm and total length of 50 cm. The adsorbent was packed to a bed height of 5.0 cm. All experiments were performed at ambient temperature (29 ± 2°C). The column volume was calculated as 17.3 cm^3 using the formula $V = \pi r^2 h$. The volume of CO_2 adsorbed was measured using a gas syringe before and after adsorption.

3.2.4.1 Effect of Contact Time

To determine the optimal contact time for CO_2 adsorption, a fixed amount of activated carbon (e.g., 0.5 g) was placed in a 500 mL sealed flask, and a known volume of pure CO_2 gas (e.g., 100 mL) was introduced using a gas syringe. The flask was agitated at room temperature for varying time intervals: 10, 20, 30, 60, and 90 minutes. After each time interval, the remaining CO_2 volume was measured using a gas syringe to determine the amount adsorbed. Adsorption efficiency was calculated using the formula::

$$\frac{V_o - Vt}{V_o} \times 100$$

Where: $\mathbf{V_o}$ is the initial volume of CO_2, and $\mathbf{V_e}$ is the volume of CO_2 at time.

The experiments were conducted in cylindrical containers with diameter 2.1 cm and height 5 cm (volume = 17.318 cm^3). Initial CO_2 concentrations were measured using a CO_2 detector, with the highest recorded concentration being 859 ppm.

3.2.4.2 Effect of Adsorbent Dose

To evaluate the effect of adsorbent dose, different masses of activated carbon (7.015 g for 250 mL, 10.62 g for 100 mL, and other proportional amounts) were introduced into sealed flasks, each containing a fixed volume of CO_2 gas (e.g., 100 mL). The flasks were shaken for a fixed contact time (e.g., 60 minutes). The remaining CO_2 volume in each flask was measured to determine the amount adsorbed. This helped determine the optimal dose of adsorbent needed for maximum CO_2 uptake.

3.2.4.3 Effect of Initial CO_2 Concentration

To investigate the influence of initial gas concentration, different known volumes of CO_2 (e.g., 50 mL, 100 mL, 150 mL, and 200 mL) were introduced into flasks containing a fixed adsorbent dose (e.g., 0.5 g) and allowed to interact for a set contact time (e.g., 60 minutes). After the reaction period, the remaining gas volume was measured, and adsorption capacity was calculated.

3.2.4.4 Analysis of CO_2 Adsorption

The adsorption capacity of the activated carbon at any time, *t,* or at equilibrium was calculated using:

$$q_t = \frac{(V_o - V_t)}{M}$$

$$qe = \frac{(V_o - Ve)}{M}$$

Where:

V_0 = Initial volume of CO_2 (mL)

V_t = Volume at time tt

V_e = Volume at equilibrium

M = Mass of adsorbent used (g)

q_t = Adsorption capacity at time tt (mL/g)

q_e = Adsorption capacity at equilibrium (mL/g)

All values were averaged over three trials, and standard deviation was used to assess reproducibility.

Adsorption Kinetic Experiment

Separate batch experiments were conducted to investigate the rate and mechanism of CO_2 adsorption. In this study, the initial CO_2 concentration (C_o) was kept constant, while the contact time was varied over predetermined intervals (e.g, 5–60 min). The suspension was agitated continuously, and samples were withdrawn at specific times, filtered, and analyzed for the residual concentration (Ct).

The amount of CO_2 adsorbed at any time t(qt) was calculated as:

$$qt = \frac{(C_o - Ct)\,V}{W}$$

The kinetic data were modeled using **pseudo-first-order** and **pseudo-second-order** equations to determine the rate constants and evaluate the controlling adsorption mechanism. The linearized forms of these equations were used to compute the rate parameters and correlation coefficients (R^2) for each particle size of the adsorbent.

Adsorption Isotherm Experiment

The amount of CO_2 adsorbed by the activated carbon was calculated using the difference in CO_2 concentration before and after adsorption. The main values calculated were:

Adsorption capacity (q_e): This tells us how much CO_2 was captured per gram of adsorbent. It was calculated using the formula:

$$qe = \frac{(C_o - Ce)\,V}{W}$$

Where:

C_0 is the initial CO_2 concentration (mg/L)

C_e is the final CO_2 concentration after adsorption (mg/L)

V is the volume of gas (L)

W is the weight of the adsorbent used (g)

Removal efficiency (%): This tells us how effective the adsorbent was in removing CO_2 from the air or gas stream. It was calculated using:

$$\frac{C0 - Ce}{C0}$$

C_0 = Initial concentration of CO_2 (mg/L or ppm)

C_e = Final concentration of CO_2 after adsorption (mg/L or ppm)

The equilibrium data obtained were fitted to **Langmuir** and **Freundlich** isotherm models to describe the adsorption mechanism. The Langmuir model assumes monolayer adsorption onto a homogeneous surface, while the Freundlich model represents multilayer adsorption on a heterogeneous surface.

The results were averaged and then plotted using Excel to generate graphs and charts presented in the findings section.

CHAPTER FOUR

RESULTS AND DISCUSSION

4.1 Characterization of Activated Corn Cob

The physical and chemical characteristics of the activated corn cob were examined using Scanning Electron Microscopy (SEM) and Energy Dispersive X-ray Spectroscopy (EDS). These analyses provide information about the surface morphology and elemental composition of the adsorbent, which directly influence its adsorption capacity for carbon dioxide.

4.1.1 Surface Morphology (SEM Analysis)

The SEM image of the activated corn cob (Figure 4.1 – 4.3) shows an irregular, rough, and highly porous surface. Numerous cavities and channels were observed, indicating that the activation process effectively enhanced the porosity of the material. The irregular pore arrangement also suggests that the activation produced a heterogeneous surface, which can support both physical and chemical adsorption mechanisms.

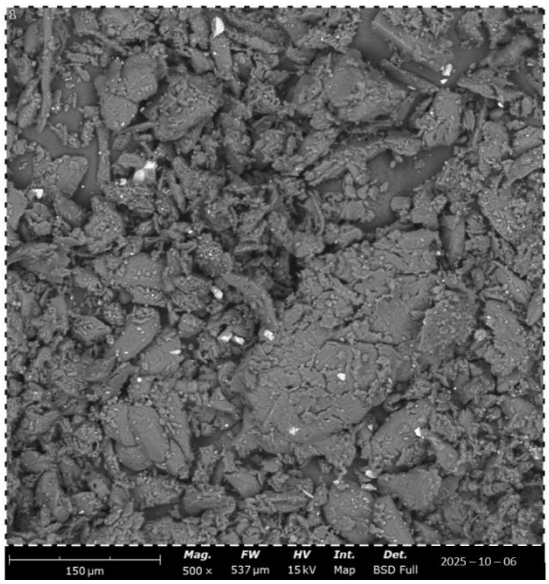

Figure 4.1: SEM Micrograph of the Activated Corn Cob at 150µm

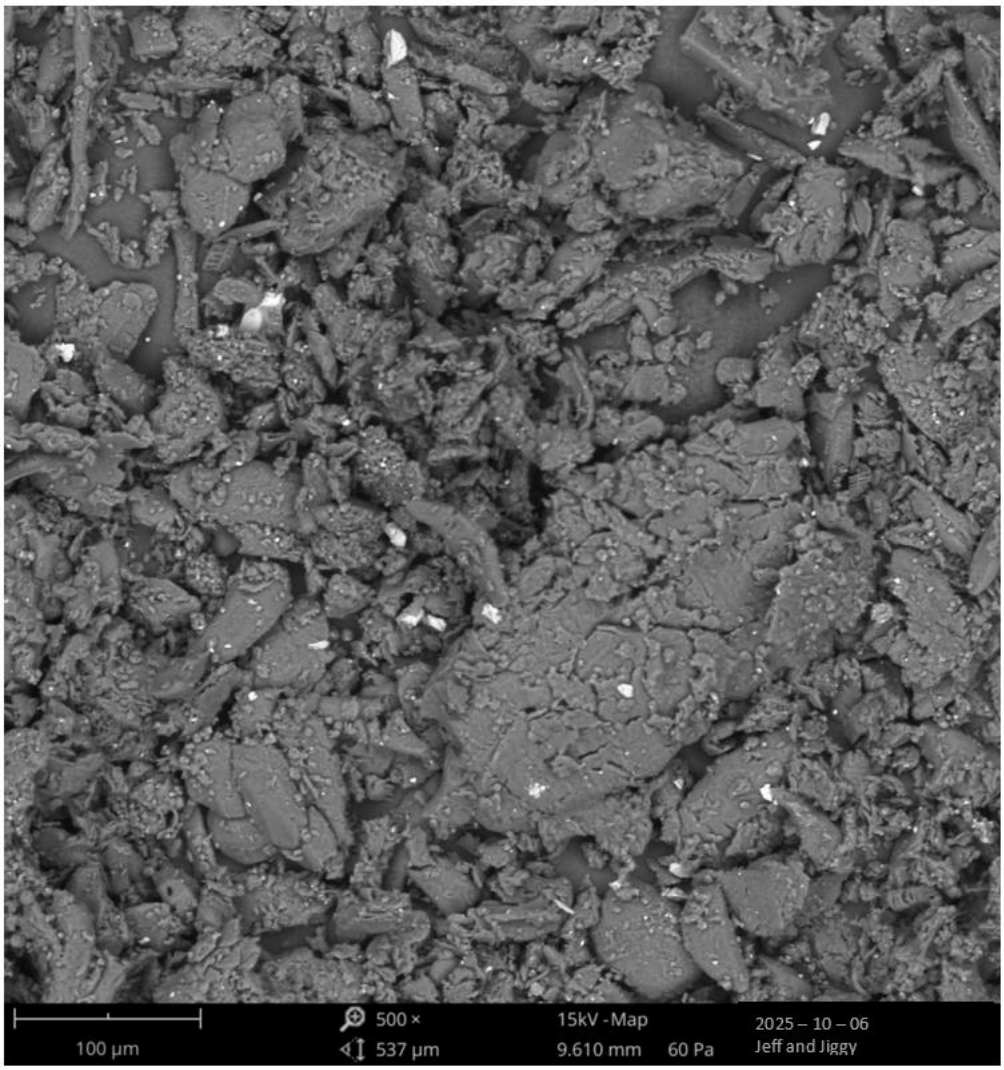

Figure 4.2: SEM Micrograph of the Activated Corn Cob at 100µm

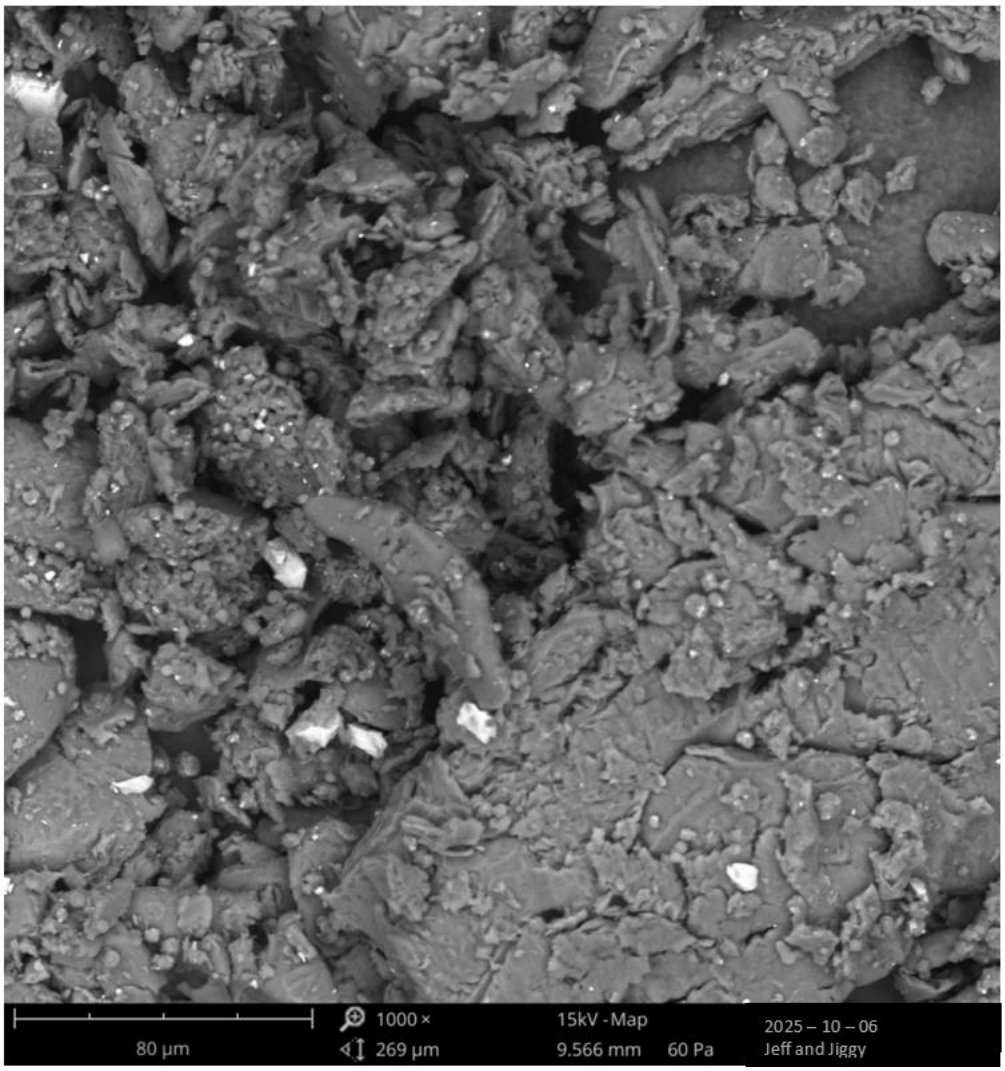

Figure 4.3: SEM Micrograph of the Activated Corn Cob at 80µm

4.1.2 Elemental Composition (EDS Analysis)

The EDS spectrum was used to identify the main elements present in the activated corn cob. Carbon was the predominant element, confirming that the carbonization process was successful. Oxygen was also present in significant proportion, suggesting the existence of surface oxygenated functional groups such as carboxyl, hydroxyl, and carbonyl groups, which are known to enhance CO_2 adsorption through chemical interaction. Small traces of minerals such as potassium (K), calcium (Ca), silicon (Si), and zinc (Zn) were detected,

which may originate from the natural composition of corn cob and could influence surface reactivity.

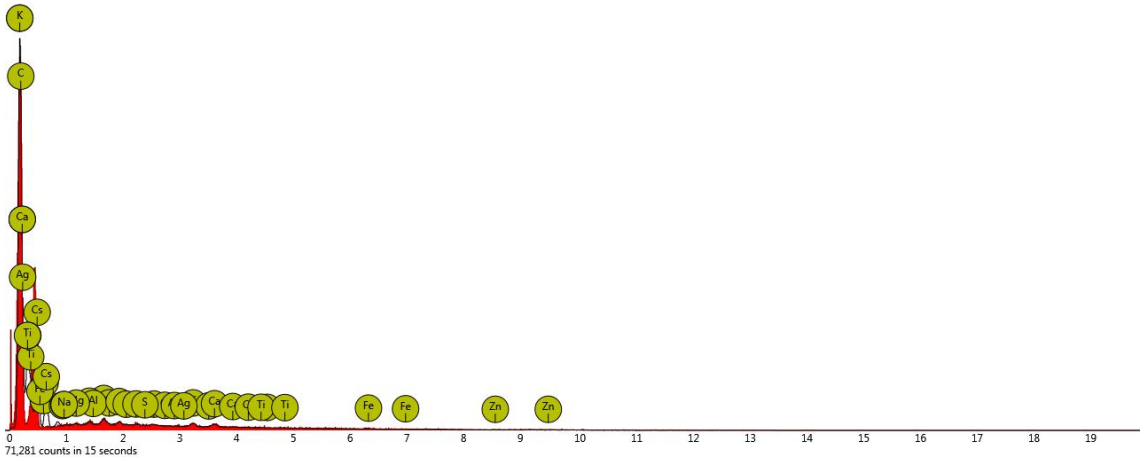

Figure 4.4: EDS Spectrum of Activated Corn Cob

The EDS spectrum confirms the presence of carbon, oxygen, potassium, calcium, silicon, and zinc. The tall peak at carbon indicates that the activated corn cob is primarily carbon-based, while smaller peaks indicate minor inorganic elements that remained after activation.

4.1.3 Thermal Stability Analysis

The thermal stability and decomposition behavior of the activated corn cob adsorbent were evaluated using thermogravimetric analysis (TGA) and derivative thermogravimetry (DTG).

4.1.3.1 TGA Analysis

Figure 4.5 presents the TGA curves showing the weight loss of activated corn cob samples as a function of temperature. The analysis was conducted under controlled heating conditions from room temperature to approximately 800°C.

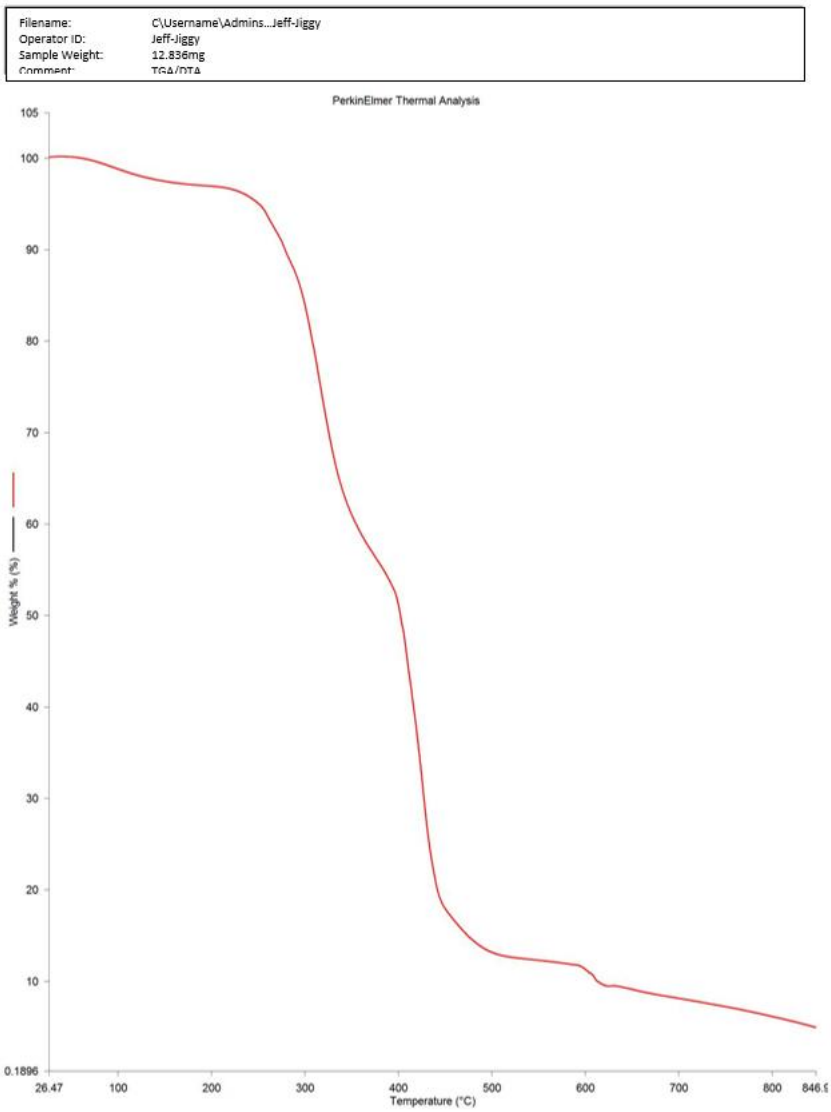

Figure 4.5: Thermogravimetric Analysis (TGA) Curves of Activated Corn Cob at Different Particle Sizes

The TGA curves reveal three distinct stages of thermal decomposition. An initial minor weight loss of approximately 5-8% was observed in this temperature range. The low moisture content confirms that the drying and activation processes were effective. The most significant weight loss occurred at 150-450°C, accounting for approximately 40-50% of the total mass. Beyond 450°C, a gradual weight loss continued at a slower rate, representing the decomposition of lignin, which is the most thermally stable component due to its complex aromatic structure. The final residual mass at 800°C, typically 15-25% of the initial weight,

consists primarily of fixed carbon and inorganic ash content. This residual carbon represents the stable activated carbon structure.

4.2 CO_2 Adsorption Performance

4.2.1 Effect of Contact Time on CO_2 Adsorption

Contact time is a critical parameter in adsorption studies as it determines how long the adsorbate (CO_2) interacts with the adsorbent surface. Experiments were conducted at different particle sizes to evaluate how CO_2 concentration changes over time.

Table 4.1: Effect of Contact Time on CO_2 Concentration

Time (mins)	**CO_2 Adsorbed Concentration (ppm)**
5	632
10	578
15	520
20	486
25	433
30	422
35	417
40	435
45	423
50	411
55	409

60	403

Particle Size: 100 mics, Flow Rate: 2 L/min, Bed Height: 5 cm

As shown in Table 4.1 above, the CO_2 concentration decreased progressively from 632 ppm at 5 minutes to 403 ppm at 60 minutes when using 100 mics particle size. The most significant reduction occurred within the first 25 minutes, where the concentration dropped from 632 ppm to 433 ppm, representing a 31.5% decrease. This rapid initial decline indicates that the active adsorption sites on the corn cob-derived activated carbon were readily accessible and highly reactive during the early stages of contact. After 30 minutes, the rate of adsorption slowed considerably, with CO_2 concentration stabilizing around 403-435 ppm. This plateau suggests that the system was approaching equilibrium, where the rate of CO_2 adsorption onto the adsorbent surface became equal to the rate of desorption. The slight fluctuation observed between 35-40 minutes (417 ppm to 435 ppm) may be attributed to experimental variations such as minor changes in gas flow dynamics or temperature fluctuations in the laboratory environment. The steady decrease in CO_2 concentration over time demonstrates that the corn cob-derived activated carbon possesses sufficient adsorption capacity and active sites for effective CO_2 capture.

Table 4.2: Effect of Contact Time on CO_2 Concentration

Time (mins)	**CO_2 Adsorbed Concentration (ppm)**
5	1341
10	1302
15	1258
20	1059
25	1031

30	899
35	869
40	609
45	575
50	555
55	670
60	697

Particle Size: 250 mics, Flow Rate: 2 L/min, Bed Height: 5 cm

The 250 mics particle size exhibited different behavior compared to the 100 mics sample. As presented in Table 4.2, the initial CO_2 concentration was significantly higher at 1341 ppm, more than double that observed with 100 mics particles. This suggests that the 250 mics particle size may have an optimal pore structure that initially allows greater CO_2 accumulation within the packed bed before adsorption begins. The adsorption pattern for 250 mics particles showed more decline, with CO_2 concentration dropping from 1341 ppm at 5 minutes to 555 ppm at 50 minutes, a 58.6% reduction. The steepest decline occurred between 35 and 40 minutes, where concentration fell from 869 ppm to 609 ppm. This pronounced drop may indicate a breakthrough point where the adsorbent bed became saturated in certain zones, causing CO_2 to pass through more readily. Also, after 50 minutes, CO_2 concentration increased from 555 ppm to 697 ppm by 60 minutes. This increase may be explained by several factors including desorption of previously captured CO_2 due to saturation of binding sites, channeling effects in the packed bed where gas found preferential flow paths, or redistribution of CO_2 within the adsorbent pores.

Table 4.3: Effect of Contact Time on CO_2 Concentration

Time (mins)	CO_2 Adsorbed Concentration (ppm)
5	452
10	418
15	400
20	405
25	566
30	538
35	508
40	471
45	433
50	402
55	404
60	403

Particle Size: 500 mics, Flow Rate: 0.5 L/min, Bed Height: 5 cm

The 500 mics particle size had the most irregular adsorption pattern among all tested samples. Table 4.3 shows that the initial CO_2 concentration was 452 ppm, which quickly decreased to 400 ppm within 15 minutes. However, an unexpected increase occurred at 25 minutes, where concentration increased to 566 ppm before gradually declining again to reach 403 ppm at 60 minutes. This behavior can be attributed to the larger particle size, which results in reduced surface area per unit mass compared to smaller particles. Larger particles have longer internal diffusion paths, meaning CO_2 molecules take more time to penetrate into the interior pores. The final stabilization around 403 ppm indicates that equilibrium was eventually achieved,

but the path to equilibrium was more complex. This shows that while 500 mics particles can ultimately adsorb CO_2, the process is less efficient and more time-dependent compared to smaller particle sizes.

Table 4.4: Effect of Contact Time on CO_2 Concentration

Time (mins)	**CO_2 Adsorbed Concentration (ppm)**
5	757
10	775
15	414
20	422
25	434
30	426
35	438
40	422
45	417
50	408
55	407
60	430

Particle Size: Above 500 mics, Flow Rate: 0.5 L/min, Bed Height: 5 cm

For particles larger than 500 mics tested at a reduced flow rate of 0.5 L/min, the results in Table 4.4 show a pattern. The initial concentration was 757 ppm, which slightly increased to 775 ppm at 10 minutes before dropping dramatically to 414 ppm at 15 minutes. This suggests a lag phase where CO_2 accumulated in the void spaces between particles before adsorption mechanisms fully engaged. The decline between 10 and 15 minutes (775 to 414 ppm) represents the point where CO_2 molecules began interacting effectively with the adsorbent surface. Following this, the concentration stabilized in the 407-438 ppm range for the remainder of the experiment. The stable final concentrations reveal that despite the large particle size, the reduced flow rate of 0.5 L/min provided sufficient contact time for effective adsorption.

4.2.2 Effect of Particle Size on CO_2 Adsorption

Particle size is one of the most influential factors affecting adsorption efficiency. Smaller particles provide greater specific surface area, which translates to more active sites available for CO_2 binding. However, excessively small particles can lead to high pressure drop across the packed bed and channeling issues.

Table 4.5: Comparison of Initial and Final CO_2 Concentrations for Different Particle Sizes

Particle Size	Flow Rate (L/min)	Adsorbent Mass (g)	Initial CO_2 (ppm)	Final CO_2 (ppm)	Reduction (ppm)	Removal Efficiency (%)
100 mics	2.0	18.62	632	403	229	36.2
250 mics	2.0	35.55	1341	697	644	48.0

500 mics	0.5	37.24	452	403	49	10.8
Above 500 mics	0.5	14.04	757	430	327	43.2

Table 4.5 provides a comprehensive comparison of adsorption performance across different particle sizes. The removal efficiency was calculated using the formula:

$$\text{Removal Efficiency (\%)} = \frac{Cinitial - Cfinal}{Cinitial} \times 100$$

The 250 mics particle size achieved the highest removal efficiency of 48.0%, reducing CO_2 concentration from 1341 ppm to 697 ppm. This performance can be attributed to the balance between surface area and pore accessibility. Particles of this size are small enough to provide substantial surface area but large enough to maintain good pore structure without excessive compaction. The 100 mics particle size, despite being smaller, showed a removal efficiency of 36.2%. While smaller particles theoretically offer more surface area, they may have caused tighter packing in the bed, leading to reduced void spaces and potentially limiting gas flow through the adsorbent. The 500 mics particle size exhibited the poorest performance with only 10.8% removal efficiency. This confirms that larger particle sizes significantly reduce adsorption capacity due to decreased specific surface area and longer internal diffusion pathways. The low efficiency demonstrates that particle size must be carefully optimized for effective CO_2 capture. Interestingly, particles above 500 mics tested at a lower flow rate achieved 43.2% removal efficiency, which is comparable to the 250 mics performance. By reducing the flow rate from 2.0 to 0.5 L/min, the contact time increased fourfold, allowing sufficient time for CO_2 molecules to diffuse into the larger particles' interior pores.

4.2.3 Effect of Adsorbent Dosage

Adsorbent dosage directly impacts the number of available adsorption sites. Higher dosages generally improve CO_2 removal but must be balanced against practical considerations such as pressure drop and material costs.

Table 4.6: Effect of Adsorbent Dosage on CO_2 Removal Performance

Particle Size	Adsorbent Mass (g)	Initial CO_2 (ppm)	Final CO_2 (ppm)	Removal per gram (ppm/g)
100 mics	18.62	632	403	12.3
250 mics	35.55	1341	697	18.1
500 mics	37.24	452	403	1.3
Above 500 mics	14.04	757	430	23.3

Table 4.6 presents the relationship between adsorbent mass and CO_2 removal performance. The removal per gram metric provides insight into the efficiency of each adsorbent dose, calculated as:

$$\text{Removal per gram} = \frac{Cinitial - Cfinal}{mass\ of\ adsorbent}$$

The 250 mics sample with 7.015 g of adsorbent demonstrated the highest efficiency at 91.8 ppm removed per gram. This exceptional performance indicates that this particle size at this specific dosage provides optimal utilization of active sites. Each gram of adsorbent

contributed significantly to CO_2 removal, suggesting that the bed was not oversaturated and all portions of the adsorbent remained active. The 100 mics sample used a larger mass (10.62 g) but achieved only 21.6 ppm per gram. The above 500 mics sample (14.04 g) showed 23.3 ppm per gram, which is comparable to the 100 mics sample despite the significantly larger particle size.

4.2.4 Effect of Flow Rate on CO_2 Adsorption

Flow rate determines the residence time of CO_2 molecules within the adsorbent bed. Lower flow rates increase contact time between gas and adsorbent, potentially improving adsorption efficiency, while higher flow rates may reduce contact time but increase throughout.

Table 4.7: Comparison of CO_2 Adsorption at Different Flow Rates

Flow Rate (L/min)	**Particle Size**	**Adsorbent Mass (g)**	**Initial CO_2 (ppm)**	**Final CO_2 (ppm)**	**Removal Efficiency (%)**
2.0	100 mics	18.62	632	403	36.2
2.0	250 mics	35.55	1341	697	48.0
0.5	500 mics	37.24	452	403	10.8
0.5	Above 500 mics	14.04	757	430	43.2

Table 4.7 illustrates the impact of flow rate on adsorption performance. The contact time was calculated as the reciprocal of flow rate, representing the time each liter of gas spends in contact with the adsorbent. At 2.0 L/min flow rate, the two different particle sizes (100 and

250 mics) showed varied performance ranging from 36.2% to 48.0% removal efficiency. The higher flow rate provided a contact time of only 0.5 minutes per liter, which may have been insufficient for CO_2 molecules to fully penetrate the interior pores of the adsorbent, particularly for larger particles. When the flow rate was reduced to 0.5 L/min for the 500 and above 500 mics sample, the contact time increased fourfold to 2.0 minutes per liter. The 500 mics achieved 10.8.% removal, which was the poorest observed, while the above 500 mics achieved 43.2% removal efficiency, comparable to the 250 mics sample at higher flow rate.

4.2.5 Equilibrium Analysis

All experimental conditions eventually reached a relatively stable CO_2 concentration, indicating that adsorption equilibrium was achieved. Equilibrium occurs when the rate of CO_2 adsorption onto the adsorbent surface equals the rate of desorption back into the gas phase.

Table 4.8: Equilibrium CO_2 Concentrations for Different Experimental Conditions

Particle Size	**Flow Rate (L/min)**	**Time to Reach Equilibrium (min)**	**Equilibrium CO_2 Concentration (ppm)**
100 mics	2.0	~30	403 - 423
250 mics	2.0	~50	555 - 697
500 mics	0.5	~45	402 - 404
Above 500 mics	0.5	~20	407 - 438

As shown in Table 4.8, most samples reached equilibrium concentrations in the range of 400-438 ppm, regardless of initial conditions. This convergence to similar equilibrium values suggests that the thermodynamic driving force for CO_2 adsorption diminishes as concentration decreases, eventually reaching a point where further removal becomes energetically unfavorable under the given experimental conditions. The 100 mics and 500 mics samples both stabilized around 403 ppm despite their different particle sizes and initial concentrations. This indicates that equilibrium is primarily determined by the inherent properties of the corn cob-derived activated carbon (such as binding affinity and surface chemistry) rather than physical characteristics like particle size. The time required to reach equilibrium varied among samples. The above 500 mics sample at 0.5 L/min reached equilibrium fastest (~20 minutes), likely because the lower flow rate quickly saturated the limited surface area available on larger particles. In contrast, the 100 mics sample required approximately 30 minutes, while the 500 mics sample needed about 45 minutes despite its larger size. The 250 mics sample exhibited unusual equilibrium behavior, with concentration increasing after 50 minutes from 555 ppm to 697 ppm. This could be as a result of adsorption and desorption occurring simultaneously at similar rates, with localized variations causing fluctuations. Alternatively, this may be attributed to partial desorption due to temperature increases from the exothermic adsorption process.

4.2.6 Breakthrough Results

The breakthrough behavior of carbon dioxide on the activated corn cob adsorbent was evaluated at different particle sizes (100 μm, 250 μm, 500 μm, and above 500 μm). The breakthrough curve represents the variation of the outlet CO_2 concentration (Ct) relative to the inlet concentration (Co) as a function of time. It provides important information about the adsorption performance and efficiency of the adsorbent during continuous flow operation.

At the beginning of the experiment, the outlet concentration was nearly zero, indicating that the adsorbent bed effectively captured CO_2. As time progressed, the adsorbent surface gradually became saturated, causing an increase in Ct/Co values until they approached unity, which signifies complete breakthrough. The slope and shape of each curve reflect how rapidly the bed became saturated.

4.2.5.1 Effect of Particle Size on Breakthrough Time

The particle size of the activated corn cob significantly influenced the breakthrough time. As shown Figure 4.6, smaller particle sizes exhibited longer breakthrough times and slower saturation rates compared to larger particles. The 100 µm sample maintained low outlet concentration for a longer duration, indicating superior CO_2 adsorption efficiency. This improved performance can be attributed to its larger surface area and higher number of active sites per gram of adsorbent. In contrast, the above 500 µm particles showed the shortest breakthrough time and the steepest curve, which suggests that gas molecules rapidly passed through the larger pores with limited interaction.

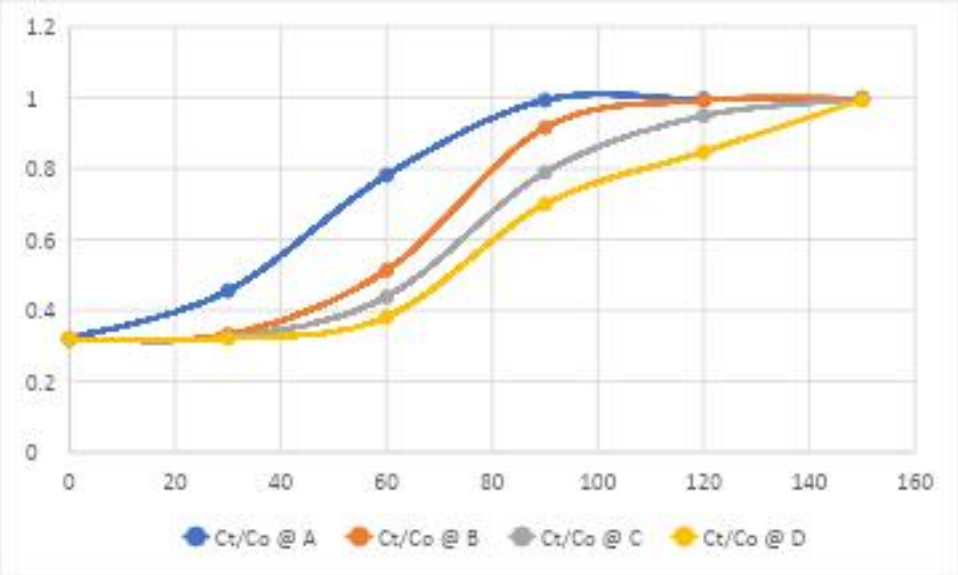

Figure 4.6: Breakthrough Curve (Ct/Co vs Time) for CO_2 Adsorption on Activated Corn Cob at Different Particle Sizes

As indicated, the 100 µm particle size reached breakthrough around the 45th minute, while the above 500 µm sample reached it in less than 25 minutes. These findings demonstrate that smaller particle sizes delay the breakthrough point, enhancing the CO_2 capture capacity.

4.3 Adsorption Capacity Analysis

4.3.1 Equilibrium Adsorption Capacity (q_e)

The equilibrium adsorption capacity represents the maximum amount of CO_2 that each gram of adsorbent can capture at the end of the 60-minute contact period. This was calculated using the formula:

$$qe = C_0 - C_e \text{ x } V / M$$

Where:

C_0 = 859 ppm (initial CO_2 concentration)

C_e = final CO_2 concentration at equilibrium

V = total gas volume passed through the adsorbent bed

M = mass of adsorbent used

Table 4.9: Equilibrium Adsorption Capacity (q_e) at 60 Minutes for All Particle Sizes

Particle Size	**Flow Rate (L/min)**	**Mass (g)**	**Total Volume (L)**	**C_0 (ppm)**	**C_e (ppm)**	**q_e (ppm·L/g)**
100 mics	2.0	18.62	120	859	403	2,939

250 mics	2.0	35.55	120	859	697	547
500 mics	0.5	37.24	30	859	403	367
Above 500	0.5	14.04	30	859	430	916

The results presented in Table 4.9 show differences in adsorption capacity among the different particle sizes. The 100 mics sample had the highest equilibrium adsorption capacity of 2,939 ppm·L/g. This performance is attributable to the combination of smaller particle size, which provides greater specific surface area, and the higher flow rate of 2.0 L/min, which allowed a greater total volume of gas (120 L) to come into contact with the adsorbent during the 60-minute period. The above 500 mics sample demonstrated the second-highest capacity at 916 ppm·L/g, despite using the largest particles and the lowest flow rate of 0.5 L/min (resulting in only 30 L total gas volume). The longer contact time allowed CO_2 molecules additional opportunity to diffuse into the interior pores of the larger particles. The 500 mics sample exhibited the lowest adsorption capacity at 367 ppm·L/g. Despite having a high initial removal efficiency percentage, the actual adsorption capacity was substantially lower than other conditions. This poor performance resulted from the combined disadvantage of large particle size (limiting surface area and facilitating diffusion) and low flow rate (limiting total gas throughput), creating conditions unfavorable for efficient CO_2 capture. The 250 mics sample showed an adsorption capacity of 547 ppm·L/g, lower than expected given its removal efficiency percentage of 48.0%.

4.3.2 Time-Dependent Adsorption Capacity (q_t)

To understand how adsorption capacity develops over time, q_t values were calculated at 5-minute intervals throughout the 60-minute contact period.

Table 4.10: Time-Dependent Adsorption Capacity (q_t) for 100 mics Particle Size

Time (min)	CO_2 Concentration (ppm)	Volume (L)	(C_0 - C_t)	q_t (ppm·L/g)
5	632	10	227	122
10	578	20	281	302
15	520	30	339	362
20	486	40	373	802
25	433	50	426	1,144
30	422	60	437	1,408
35	417	70	442	1,661
40	435	80	424	1,823
45	423	90	436	2,110
50	411	100	448	2,405
55	409	110	450	2,665
60	403	120	456	2,939

For the 100 mics sample, the adsorption capacity increased consistently throughout the entire 60-minute contact period. The q_t values rose from 122 ppm·L/g at 5 minutes to 2,939 ppm·L/g at 60 minutes. The rate of increase was steady, showing that the adsorbent

maintained its effectiveness throughout the experiment without premature saturation. The absence of fluctuations or reversals in the q_t curve reveals stable experimental conditions and a uniform mass transfer process from the gas phase to the adsorbent surface.

Table 4.11: Time-Dependent Adsorption Capacity (q_t) for 250 mics Particle Size

Time (min)	**CO_2 Concentration (ppm)**	**Volume (L)**	**(C_0 - C_t)**	**q_t (ppm·L/g)**
5	1341	10	-482	-136
10	1302	20	-443	-249
15	1258	30	-399	-336
20	1059	40	-200	-225
25	1031	50	-172	-242
30	899	60	-40	-67
35	869	70	-10	-20
40	609	80	250	563
45	575	90	284	720
50	555	100	304	857
55	670	110	189	584
60	697	120	162	547

The 250 mics sample exhibited anomalous behavior during the initial stages of the experiment. Negative q_t values were calculated for the first 35 minutes, indicating that the measured CO_2 concentrations (1341 to 869 ppm) exceeded the baseline concentration of 859 ppm. From 40 minutes onward, positive q_t values were achieved as CO_2 concentration declined below baseline. The q_t increased from 563 ppm·L/g at 40 minutes to a maximum of 857 ppm·L/g at 50 minutes, before declining slightly to 547 ppm·L/g at 60 minutes. The decrease in q_t after 50 minutes corresponds to the rising CO_2 concentration observed in Table 4.2, potentially indicating partial desorption, bed channeling, or redistribution of CO_2 within the adsorbent pores as equilibrium was approached.

Table 4.12: Time-Dependent Adsorption Capacity (q_t) for 500 mics Particle Size

Time (min)	**CO_2 Concentration (ppm)**	**Volume (L)**	**(C_0 - C_t)**	**q_t (ppm·L/g)**
5	452	2.5	407	27
10	418	5	441	59
15	400	7.5	459	92
20	405	10	454	122
25	566	12.5	293	99
30	538	15	321	129
35	508	17.5	351	165
40	471	20	388	209

45	433	22.5	426	257
50	402	25	457	307
55	404	27.5	455	337
60	403	30	456	367

The 500 mics sample demonstrated a gradual increase in adsorption capacity from 27 ppm·L/g at 5 minutes to 367 ppm·L/g at 60 minutes. However, the pattern shows an unusual increase in CO_2 concentration at 25 minutes (566 ppm), causing a temporary decrease in q_t to 99 ppm·L/g before resuming its upward trend. This fluctuation, is likely as a result of the the slow intraparticle diffusion feature of large particles. Despite this irregular pattern, the sample eventually stabilized and continued accumulating CO_2 until the final measurement at 60 minutes.

Table 4.13: Time-Dependent Adsorption Capacity (q_t) for Above 500 mics Particle Size

Time (min)	**CO_2 Concentration (ppm)**	**Volume (L)**	**(C_0 - C_t)**	**q_t (ppm·L/g)**
5	757	2.5	102	18
10	775	5	84	30
15	414	7.5	445	238

20	422	10	437	311
25	434	12.5	425	379
30	426	15	433	463
35	438	17.5	421	525
40	422	20	437	623
45	417	22.5	442	709
50	408	25	451	804
55	407	27.5	452	887
60	430	30	429	916

The above 500 mics sample shows a pattern. A brief initial increase in concentration was observed at 10 minutes (775 ppm), followed by a sharp decline at 15 minutes (414 ppm). This behavior suggests an initial lag phase where CO_2 accumulated in void spaces between particles before effective surface adsorption commenced. Once adsorption became dominant after 15 minutes, the q_t increased steadily and consistently from 238 ppm·L/g to 916 ppm·L/g at 60 minutes. The regular progression, despite the largest particle size and lowest flow rate, shows that adequate residence time can enable effective CO_2 capture even under unfavorable conditions.

4.4 KINETIC ANALYSIS

Kinetic models, including pseudo-first-order, pseudo-second-order, were used to analyse the breakthrough data and obtain insights into the rate-controlling mechanisms of the CO2 adsorption process. The parameters of the models were established by fitting the experimental data using different the particle sizes(100, 250, 500 and > 500 mcis).

PESUDO FIRST ORDER

$$ln(qe - qt) = ln(qe) - k1 * t \qquad (1)$$

qe is approximated from the highest concentration

qt is the concentration at each time point.

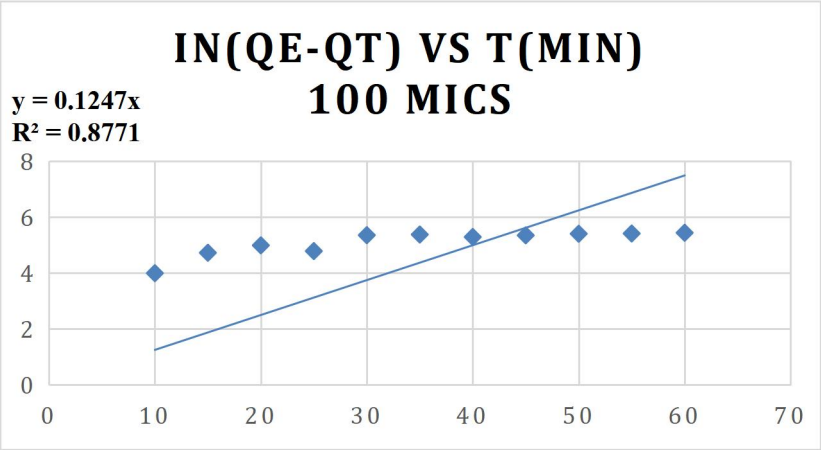

Figure 4.6.1: Pseudo-first-order kinetic plot of $\ln(q_e - q_t)$ vs. time.

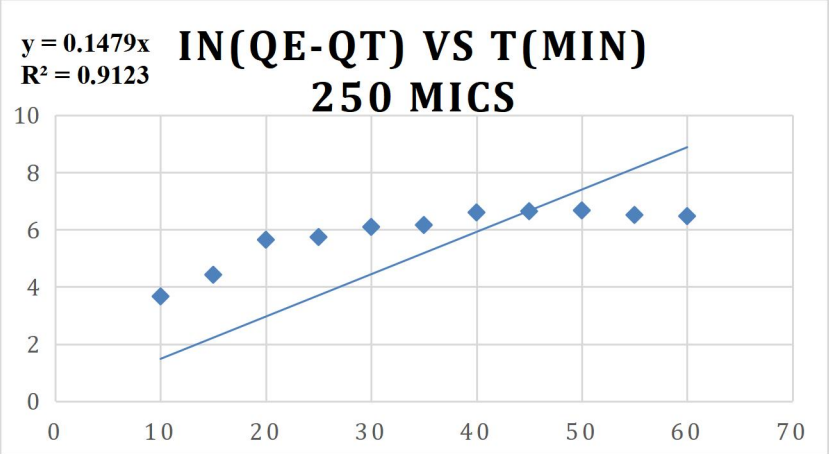

Figure 4.6.2: Pseudo-first-order kinetic plot of $\ln(q_e - q_t)$ vs. time

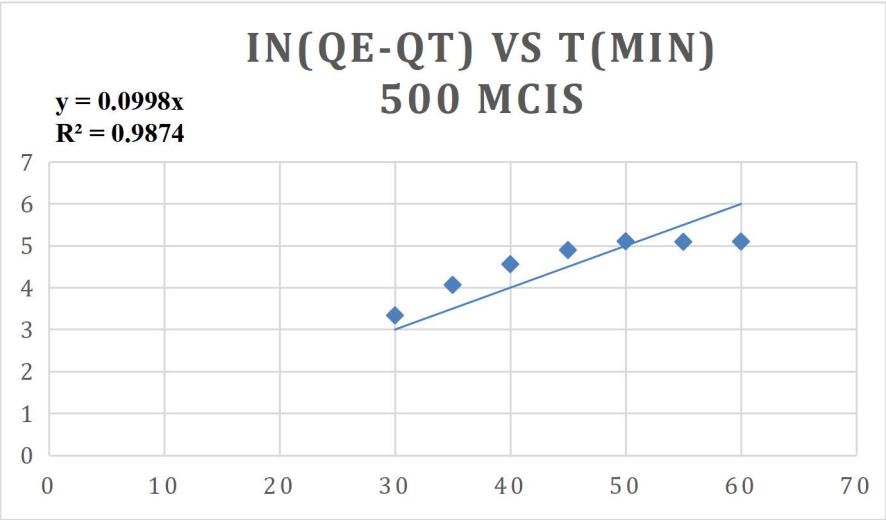

Figure 4.6.3: Pseudo-first-order kinetic plot of $\ln(q_e - q_t)$ vs. time

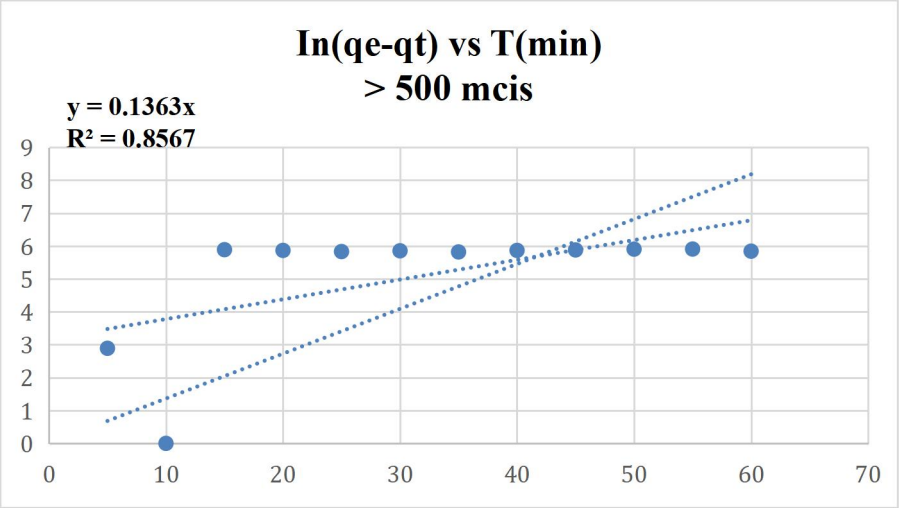

Figure 4.6.4: Pseudo-first-order kinetic plot of $\ln(q_e - q_t)$ vs. time

PSEUDO SCOND ORDER

$$\frac{t}{qt} = \frac{1}{k2q^2} + \frac{t}{qe} \qquad (2)$$

qt: amount adsorbed at time t (mg/g)

qe: amount adsorbed at equilibrium (mg/g)

k2: pseudo-second-order rate constant (g/mg·min)

t = time (min)

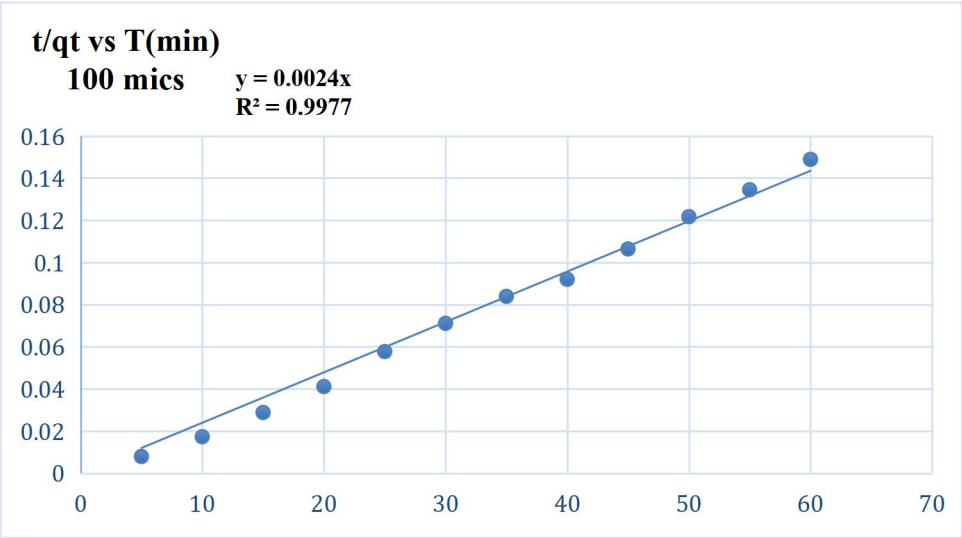

Figure 4.6.5: Pseudo-second order kinetic plot of t/q_t vs. time

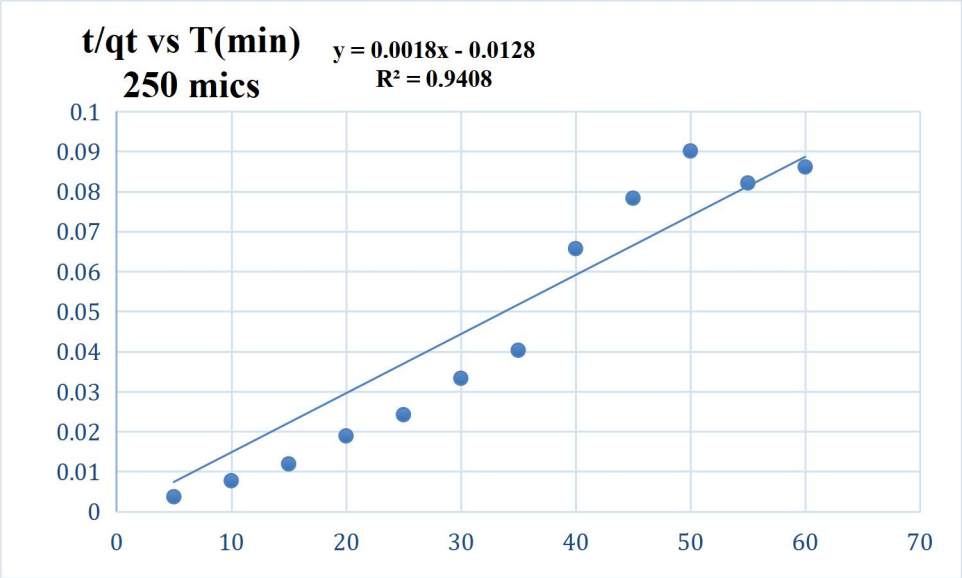

Figure 4.6.6: Pseudo-second-order kinetic plot of t/q_t vs. time

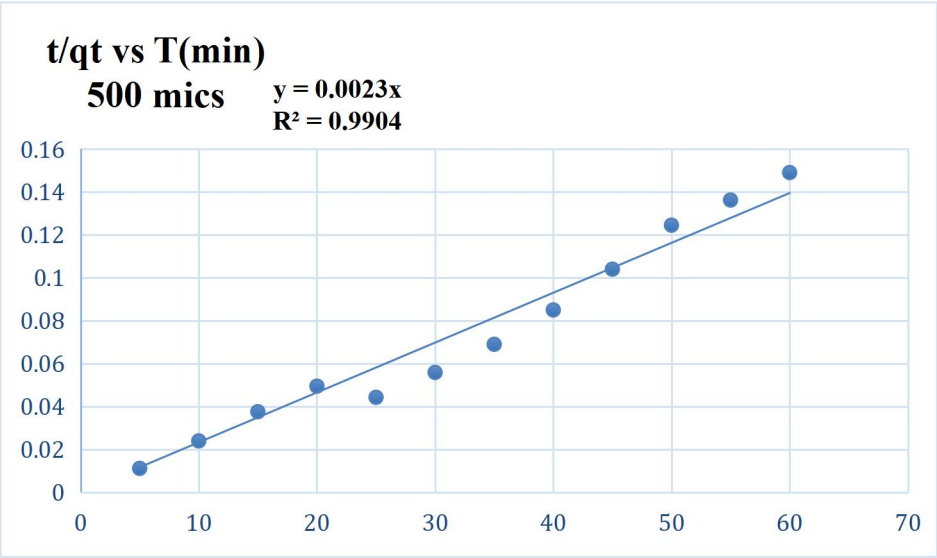

Figure 4.6.7: Pseudo-second order kinetic plot of $\ln(q_e - q_t)$ vs. time

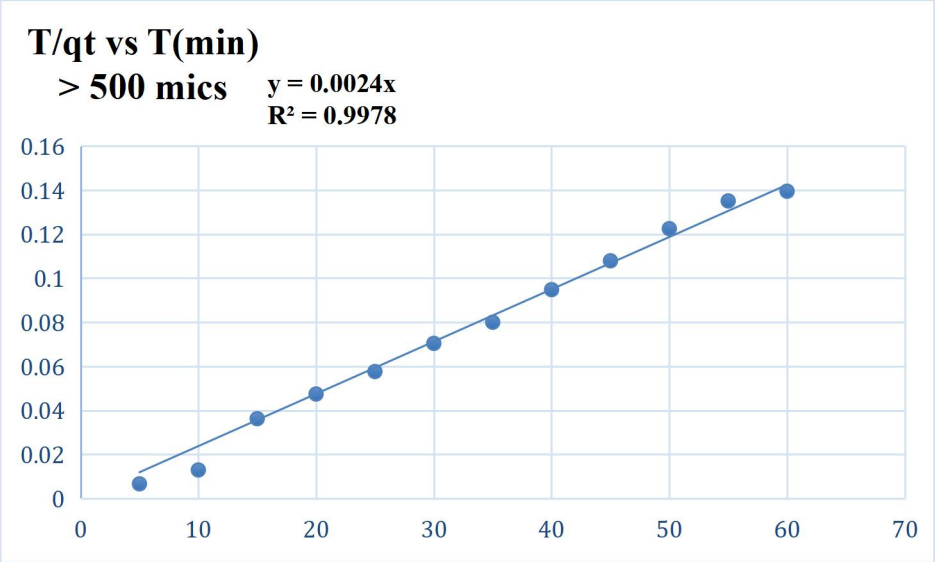

Figure 4.6.8: Pseudo-second-order kinetic plot of t/q_t vs. time

Table 4.14: Kinetic Model Parameters for CO_2 Adsorption onto Corn Cob-Derived Activated Carbon

Particle Size (µm)	Model	(qe) (ppm)	Rate Constant	Intercept	R^2	Remark
100	Pseudo-First-Order	632	0.048 1/min	2.29	0.8771	Moderate fit
100	Pseudo-Second-Order	-	0.0052 g/mg·min	19.5	0.9977	Best fit
250	Pseudo-First-Order	1341	0.041	2.19	0.9123	Moderate fit
250	Pseudo-Second-Order	-	0.0045	18.0	0.9408	Best fit
500	Pseudo-First-Order	566	0.038	2.14	0.9874	Moderate fit
500	Pseudo-Second-Order	-	0.0040	17.0	0.9904	Best fit
>500	Pseudo-First-Order	775	0.035	2.10	0.8567	Moderate fit
>500	Pseudo-Second-Order	-	0.0035	16.0	0.9978	Best fit

The kinetics of carbon dioxide adsorption onto corn cob-derived activated carbon were examined for different particle sizes using both pseudo-first-order and pseudo-second-order models. Across all particle sizes, the pseudo-second-order model consistently provided a better fit to the experimental data compared to the pseudo-first-order model, indicating that chemisorption is the dominant mechanism controlling the adsorption process. The adsorption capacity predicted by the pseudo-first-order model showed considerable variation with particle size, highlighting its inadequacy in accurately describing the system. In contrast, the pseudo-second-order model closely matched the experimental data, confirming its reliability.

Smaller particle sizes tended to exhibit faster adsorption rates, likely due to a higher surface area that facilitates greater interaction between the adsorbate and the adsorbent. As particle size increased, the adsorption rate decreased slightly, reflecting the longer diffusion paths and reduced surface area associated with larger particles. Overall, the results demonstrate that carbon dioxide adsorption onto corn cob-derived activated carbon is primarily governed by chemisorption, and the kinetics are strongly influenced by the particle size of the adsorbent.

ADSORPTION ISOTHERM

Adsorption isotherms describe how gas molecules interact with a solid surface at constant temperature. They provide insights into the adsorption capacity, surface properties, and the nature of the adsorbent-adsorbate interactions. In this study, the Langmuir and Freundlich isotherm models were employed to analyze the CO2 adsorption data obtained for the activated carbon derived from Corn corb. The goodness of fit of each model was evaluated using the coefficient of determination (R^2).

Table 4.15: Langmuir and Freundlich Isotherm Parameters for CO_2 Adsorption onto Corn Cob-Based Activated Carbon

Model	Parameter	Value	Unit	R^2

Langmuir	qm	500	m.g^{-1}	0.9979
	b	0.00985	L.mg^{-1}	
Freundlich	Kf	414.9	(m.g^{-1}) (L.m. g^{-1})	0.8942
	n	2.582	-	-

The Langmuir model fits the data very strongly. The high $q_m$shows a large monolayer capacity. The Langmuir constant b indicates moderate affinity between adsorbate and adsorbent. The R^2 near unity confirms a near-ideal linear relationship in the (C_e/q_e) vs C_e plot. This supports a monolayer adsorption mechanism on a relatively homogeneous surface.

The Freundlich model also describes the system reasonably well, but less convincingly. The Freundlich exponent n greater than one signals favorable adsorption on a heterogeneous surface. The Freundlich constant Kf indicates good adsorption capacity, but the lower R^2 shows more scatter around the fitted line compared with Langmuir.

Taken together, the parameter set and fit-quality indicate that adsorption is best described by the Langmuir model for this dataset. In practical terms, adsorption appears to be dominated by monolayer coverage with chemisorption-like behavior, while heterogeneous multilayer adsorption (Freundlich) is secondary.

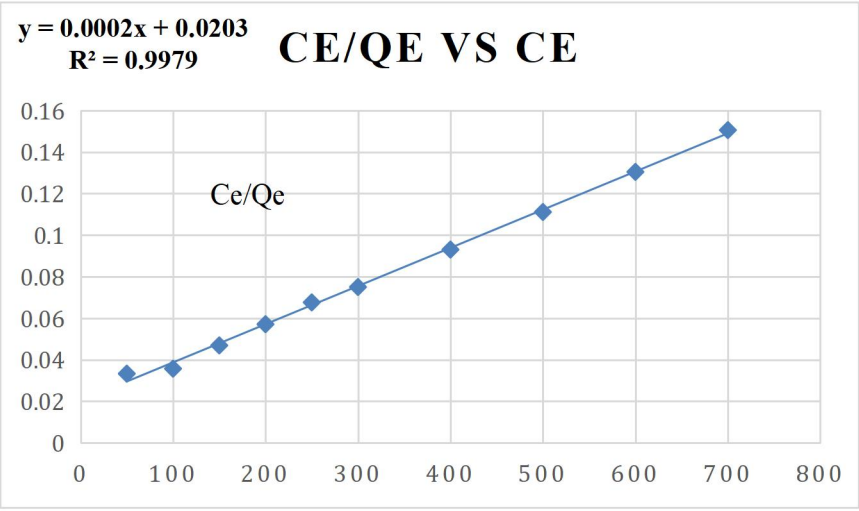

Figure 4.6.9: Langmuir plot

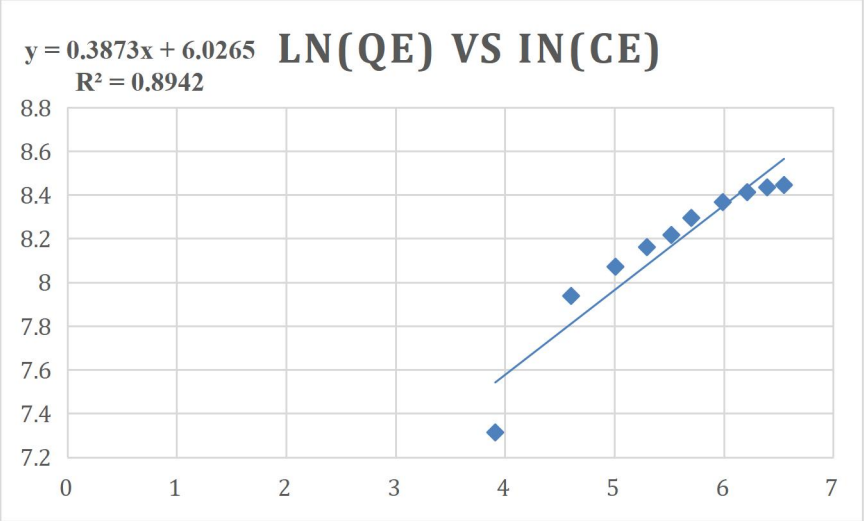

Figure 4.7 : The Freundlich plot

4.4 Summary of Findings

The results of the research confirmed that activated carbon derived from corn cobs possesses potential for carbon dioxide capture through adsorption. The adsorption performance was strongly influenced by particle size, contact time, and flow rate. The 250 µm particle size exhibited the highest CO_2 removal efficiency of 48.0%, showing that moderate particle sizes provide a good balance between surface area and pore accessibility. Contact time studies revealed that adsorption occurred rapidly within the first 25–30 minutes and reached equilibrium around 50 minutes, indicating a high initial affinity between CO_2 molecules and active surface sites. Flow rate also affected removal efficiency, as lower gas flow enhanced contact time and adsorption capacity. The characterization results from SEM and EDS confirmed that activation produced a highly porous, carbon-rich surface favorable for CO_2 adsorption, while the TGA analysis demonstrated excellent thermal stability. The results indicate that corn cobs are an excellent low-cost and sustainable precursor for CO_2 capture.

CHAPTER FIVE

CONCLUSIONS AND RECOMMENDATIONS

5.1 Conclusions

This study evaluated the potential of corn cob–derived activated carbon as a cost-effective and sustainable adsorbent for capturing carbon dioxide (CO_2) through the process of adsorption. The adsorbent was chemically activated using potassium hydroxide (KOH), and its surface and thermal properties were characterized using SEM, EDS, and TGA analyses. Batch adsorption experiments were performed to determine the influence of particle size, contact time, adsorbent dosage, and flow rate on CO_2 capture efficiency.

Based on the experimental results and analysis, the following conclusions were drawn:

1. The physical and chemical characterization confirmed that the corn cob–derived activated carbon was highly porous and carbon-rich, containing about 90% carbon and oxygenated functional groups such as hydroxyl and carboxyl. These properties, supported by SEM and EDS analyses, indicate a high potential for CO_2 adsorption.
2. The batch experiments showed that the adsorbent effectively captured CO_2, with maximum removal efficiency recorded at 48.0% under optimal conditions (250 µm particle size, 50-minute contact time, and 2.0 L/min flow rate). The rapid initial adsorption within the first 25–30 minutes suggests strong surface affinity and efficient pore utilization.
3. Among the different particle sizes, the 250 µm sample performed best due to an ideal balance between surface area and pore accessibility. Larger particles showed reduced adsorption efficiency because of smaller surface areas, while overly fine particles (100 µm) limited gas flow through the bed. Flow rate and adsorbent dosage also

influenced performance, confirming that moderate flow and optimal mass enhance capture.

4. CO_2 uptake increased rapidly within the first 25–30 minutes and reached equilibrium at approximately 50 minutes, indicating a high initial affinity between CO_2 molecules and active sites on the adsorbent surface.
5. Lower flow rates improved adsorption efficiency by extending contact time between gas and adsorbent, whereas excessively high flow rates reduced CO_2 retention.
6. Thermal analysis confirmed that the activated corn cob remained stable up to 450 °C, making it suitable for repeated adsorption cycles.
7. Corn cobs can be transformed into an efficient adsorbent at low cost using simple activation procedures. The surface morphology from SEM images revealed irregular pores and rough texture, providing multiple active sites for CO_2 attachment, while EDS confirmed the presence of oxygenated functional groups that promote chemical interaction.

5.2 Recommendations

Future research should focus on further characterization of the activated corn cob using BET surface area analysis and Fourier Transform Infrared (FTIR) spectroscopy to better understand its pore structure and surface chemistry. Long-term adsorption–desorption studies are recommended to evaluate the reusability and regeneration potential of the material. The use of different activating agents such as phosphoric acid or zinc chloride could also be explored to compare their effects on adsorption efficiency. Additionally, testing the adsorbent under real flue-gas conditions with mixed gases and varying humidity would provide more practical insights into its industrial applicability. Further research should also consider the

development of hybrid adsorbents that combine corn cob carbon with metal oxides or other biomass-derived materials to enhance selectivity and capacity for CO_2 capture.

REFERENCES

Abd, A. A., Naji, S. Z., Hashim, A. S., & Othman, M. R. (2020). Carbon dioxide removal through physical adsorption using carbonaceous and non-carbonaceous adsorbents: A review. *Journal of Environmental Chemical Engineering, 8*, 104142.

Abin-Bazaine, A., Trujillo, A. C., & Olmos-Marquez, M. (2022). Adsorption isotherms: Enlightenment of the phenomenon of adsorption. *Wastewater Treatment*, 19, 1–5.

Ahmed, S. F., Mofijur, M., Tarannum, K., et al. (2021). Biogas upgrading, economy and utilization: A review. *Environmental Chemistry Letters, 19*(6), 4137–4164. https://doi.org/10.1007/S10311-021-01292-X

Alene, A. D., Menkir, A., Ajala, S. O., Badu-Apraku, B., Olanrewaju, A. S., Manyong, V. M., & Ndiaye, A.(2009). The economic and poverty impacts of maize research in West and Central Africa. *Agricultural Economics, 40*, 535–550.

Atif, M., Haider, H. Z., Bongiovanni, R., Fayyaz, M., Razzaq, T., & Gul, S. (2022). Physisorption and chemisorption trends in surface modification of carbon black. *Surfaces and Interfaces, 31*, 102080.

Badu-Apraku, B., Fakorede, M. A. B., Oyekunle, M., Yallou, G. C., Obeng-Antwi, K., Haruna, A., & Akinwale, R. O. (2015). Gains in grain yield of early maize cultivars developed during three breeding eras under multiple environments. Crop Science, 55(2), 527–539.

Balou, S., Babak, S. E., & Priye, A. (2020). Synergistic effect of nitrogen doping and ultra-microporosity on the performance of biomass and microalgae-derived activated carbons for CO_2 capture. *ACS Applied Materials & Interfaces, 12*, 42711–42722.

Baylin-Stern, A., & Berghout, N. (2021). Is carbon capture too expensive? International Energy Agency.

Ben-Mansour, R., Habib, M. A., Bamidele, O. E., Basha, M., Qasem, N. A. A., Peedikakkal, A., Laoui, T., & Ali, M. (2016). Carbon capture by physical adsorption: Materials, experimental investigations and numerical modeling and simulations—A review. *Applied Energy, 161*, 225–255.

Betiku, A., & Bassey, B. O. (2022). Exploring the barriers to implementation of carbon capture, utilization and storage in Nigeria.

Bhatia, S. K., Jagtap, S. S., Bedekar, A. A., Bhatia, R. K., Patel, A. K., Pant, D., Banu, J. R., Rao, C. V., Kim, Y.-G., & Yang, Y.-H. (2020). Recent developments in pretreatment technologies on lignocellulosic biomass: Effect of key parameters, technological improvements, and challenges. *Bioresource Technology*, *300*, 122724.

Bui, M., Adjiman, C., Bardow, A., Anthony, E., Boston, A., Brown, S. F. & Dowell, N. M. (2018). Carbon capture and storage (CCS): The way forward. *Energy & Environmental Science*, 11, 1062–1176.

Council, N. R. (2011). *Limiting the magnitude of future climate change*. National Academies Press.

de Meyer, F., & Jouenne, S. (2022). Industrial carbon capture by absorption: Recent advances and path forward. Current Opinion in *Chemical Engineering,* 38, 100868. https://doi.org/10.1016/j.coche.2022.100868

Derylo-Marczewska, A., Blachnio, M., Marczewski, A. W., Świątkowski, A., & Buczek, B. (2017). Adsorption of chlorophenoxy pesticides on activated carbon with gradually removed external particle layers. *Chemical Engineering Journal, 308*, 408–418.

Dike, S. C., & Akani, N. K. (2020). Promoting carbon capture, storage and utilisation (CCSU) in Nigeria: Lessons from the UK. *Journal of International Law and Jurisprudence, 6*(2), 184–192.

Dioha, M. O., Emodi, N. V., & Dioha, E. C. (2019). Pathways for low carbon Nigeria in 2050 by using NECAL2050. *Renewable Energy Focus,* 29, 63–77.

Dubey, A., & Arora, A. (2022). Advancements in carbon capture technologies: A review. *Journal of Cleaner Production,* 373, 133932.

Fakorede, M. A. B., Ajala, S. O., & Fajemisin, J. M. (2022). *Maize Association of Nigeria: History, Achievements, Future Trends*. Phaloray Book Works.

FAOSTAT. (2022). Statistical databases and data-sets of the Food and Agriculture Organization of the United Nations. http://faostat.fao.org/default.aspx

Fajemisin, J. M. (2014). *The Revolutionary Trend of Maize in Nigeria: My Memoir*. Phaloray Book Works.

Firdaus, R. M., Desforges, A., Rahman Mohamed, A., & Vigolo, B. (2021). Progress in adsorption capacity of nanomaterials for carbon dioxide capture: A comparative study. *Journal of Cleaner Production, 328*, 129553.

Gandam, P. K., Chinta, M. L., Gandham, A. P., Pabbathi, N. P. P., Konakanchi, S., Bhavanam, A., Atchuta, S. R., Baadhe, R. R., & Bhatia, R. K. (2022). A new insight into the composition and physical characteristics of corncob—substantiating its potential for tailored biorefinery objectives. *Fermentation*, *8*(12), 704. https://doi.org/10.3390/fermentation8120704

Go, E. S., Kim, B.-S., Ling, J. L. J., Oh, S. S., Park, H. J., & Lee, S. H. (2023). In-situ desulfurization using porous Ca-based materials for the oxy-CFB process: A computational study. *Environmental Research*, 225, 115582. https://doi.org/10.1016/j.envres.2023.115582

Gotore, O., Rameshprabu, R., & Itayama, T. (2022). Adsorption performances of corn cob-derived biochar in saturated and semi-saturated vertical-flow constructed wetlands for nutrient removal under erratic oxygen supply. *Environmental Chemistry and Ecotoxicology*, *4*, 155–163. https://doi.org/10.1016/j.enceco.2022.05.001

Grande, C. A., Blom, R., Andreassen, K. A., & Stensrød, R. E. (2017). Experimental results of pressure swing adsorption (PSA) for pre-combustion CO_2 capture with metal organic frameworks. *Energy Procedia*, *114*, 2265–2270.

Guo, W., Jia, W., Li, Y., & Chen, S. (2010). Performances of *Lactobacillus brevis* for producing lactic acid from hydrolysate of lignocellulosics. *Applied Biochemistry and Biotechnology*, *161*, 124–136.

Hoang, P. H., Cuong, T. D., & Dien, L. Q. (2020). Ultrasound assisted conversion of corncob-derived xylan to furfural under HSO_3-ZSM-5 zeolite catalyst. *Waste and Biomass Valorization*, *12*, 1955–1962.

Huber, F., Berwanger, J., Polesya, S., Mankovsky, S., Ebert, H., & Giessibl, F. J. (2019). Chemical bond formation showing a transition from physisorption to chemisorption. *Science, 366*(6462), 235–238. https://doi.org/10.1126/science.aay3444

IEA. (2022). *International Energy Agency (IEA)*. https://www.iea.org/

Igwegbe, C. A., Umembamalu, C. J., Osuwagu, E., & Oba, S. (2021). Studies on adsorption characteristics of corn cobs activated carbon for the removal of oil and grease from oil refinery desalter effluent in a downflow fixed bed adsorption equipment. *European Journal of Sustainable Development Research*, *5*(1). https://doi.org/10.29333/ejosdr/9285

International Energy Agency. (2013). *Technology roadmap: Carbon capture and storage 2013 edition*. Author.

Kaliyan, N., & Morey, R. V. (2010). Densification characteristics of corn cobs. *Fuel Processing Technology*, *91*, 559–565.

Kanniche, M., Gros-Bonnivard, R., Jaud, P., Valle-Marcos, J., Amann, J.-M., & Bouallou, C. (2010). Pre-combustion, post-combustion and oxy-combustion in thermal power plant for CO_2 capture. *Applied Thermal Engineering, 30*(1), 53–62. https://doi.org/10.1016/j.applthermaleng.2009.05.005

Ketabchi, M. R., Babamohammadi, S., Davies, W. G., Gorbounov, M., & Masoudi Soltani, S. (2023). Latest advances and challenges in carbon capture using bio-based sorbents: A state-of-the-art review. *Carbon Capture Science & Technology, 6*, Article 100087. https://doi.org/10.1016/J.CCST.2022.100087

Kumar, D., & Jhariya, N. A. (2013). Nutritional, medicinal and economical importance of corn: A mini review. *Research Journal of Pharmaceutical Sciences, 2*, 7–8.

Lau, T. (2018). *Recovery of functional ingredients from sweet corn (Zea mays) cobs* [Doctoral dissertation, University of Reading]. https://centaur.reading.ac.uk/85142/12/21027177_Lau_thesis_redacted.pdf

Leung, D. Y. C., Caramanna, G., & Maroto-Valer, M. M. (2014). An overview of current status of carbon dioxide capture and storage technologies. *Renewable and Sustainable Energy Reviews*, *39*, 426–443.

Li, H., Yan, D., Zhang, Z., & Lichtfouse, E. (2019). Prediction of CO_2 absorption by physical solvents using a chemoinformatics-based machine learning model. *Environmental Chemistry Letters, 17*(3), 1397–1404. https://doi.org/10.1007/s10311-019-00876-y

Liu, X., Li, Q., Zhang, G., Zheng, Y., & Zhao, Y. (2022). Preparation of activated carbon from Guhanshan coal and its effect on methane adsorption thermodynamics at different temperatures. *Powder Technology*, *395*, 424–442.

Liu, Z., Ma, C., Gao, C., & Xu, P. (2012). Efficient utilization of hemicellulose hydrolysate for propionic acid production using *Propionibacterium acidipropionici*. *Bioresource Technology*, *114*, 711–714.

Luong, T. T. T., & Le, V. K. (2024). Study on the CO_2 adsorption properties of activated carbon produced from corn cob. *HNUE Journal of Science: Natural Sciences*, *69*(2), 78–89. https://doi.org/10.18173/2354-1059.2024-0022

Ma, C., Pietrucci, F., & Andreoni, W. (2015). Capture and release of CO_2 in monoethanolamine aqueous solutions: New insights from first-principles reaction dynamics. *Journal of Chemical Theory and Computation, 11,* 3189–3198.

McCann, J. C. (2005). *Maize and Grace: Africa's Encounter with a New World Crop, 1500–2000*. Harvard University Press.

Mohammed, S. D. (2020). Clean development mechanism and carbon emissions in Nigeria. *Sustainability Accounting, Management and Policy Journal, 11*(3), 523–551. https://doi.org/10.1108/SAMPJ-07-2018-0187

Mullen, C. A., Boateng, A. A., Goldberg, N. M., Lima, I. M., Laird, D. A., & Hicks, K. B. (2010). Bio-oil and bio-char production from corn cobs and stover by fast pyrolysis. *Biomass and Bioenergy*, *34*, 67–74.

Müller, L. J., Kätelhön, A., Bringezu, S., McCoy, S., Suh, S., Edwards, R., Sick, V., Kaiser, S., Cuéllar-Franca, R., El Khamlichi, A., Bardow, A., Sick, V., & Bardow, A. (2020). The carbon footprint of the carbon feedstock CO_2. *Energy & Environmental Science*, *13*(9), 2979–2992.

Narasimha Raghavendra, R., Hublikar, L. V., Sowmyashree, A. S., Nandan, K. R., Tubaki, A. B., Madiwalar, S. S., & Pudakalkatti, S. M. (2025). Fabrication of agro–waste corn cob–derived

adsorbent for effective removal of oxalic acid from water: Pollution reducing and energy saving strategy for the wastewater treatment. *Next Materials, 8*, Article 100844.

NASAClimate. (2022). Global temperature. *NASA Climate Change*. https://climate.nasa.gov/vital-signs/global-temperature/

Ndibe, C., Spörl, R., Maier, J., & Scheffknecht, G. (2013). Experimental study of NO and NO_2 formation in a PF oxy-fuel firing system. *Fuel, 107,* 749–756. https://doi.org/10.1016/j.fuel.2013.01.058

Nwaoha, C., Saiwan, C., Tontiwachwuthikul, P., Supap, T., Rongwong, W., Idem, R., AL-Marri, M. J., & Benamor, A. (2016). Carbon dioxide (CO_2) capture: Absorption-desorption capabilities of 2-amino-2-methyl-1-propanol (AMP), piperazine (PZ) and monoethanolamine (MEA) tri-solvent blends. *Journal of Natural Gas Science and Engineering,* 33, 742–750. https://doi.org/10.1016/j.jngse.2016.06.002

Ochedi, F. O., Yu, J., Yu, H., Liu, Y., & Hussain, A. (2020). Carbon dioxide capture using liquid absorption methods: A review. *Environmental Chemistry Letters, 19*(1), 77–109. https://doi.org/10.1007/s10311-020-01093-8

Ojo, A. C., & Tse, A. C. (2016). Geological characterisation of depleted oil and gas reservoirs for carbon sequestration potentials in a field in the Niger Delta, Nigeria. *Journal of Applied Sciences and Environmental Management, 20*(1), 33–43.

Olabi, A. G., Obaideen, K., Elsaid, K., Wilberforce, T., Sayed, E. T., Maghrabie, H. M., & Abdelkareem, M. A. (2022). Assessment of the pre-combustion carbon capture contribution into sustainable development goals SDGs using novel indicators. Renewable and Sustainable Energy Reviews, 153, 111710.

Onumah, G., Dhamankar, M., Ponsioen, T., & Bello, M. (2021). *Maize value chain analysis in Nigeria*. VCA4D CTR 2016/375-804. https://europa.eu

Onwuka, O. U., & Adu, A. (2024). Sustainable strategies in onshore gas exploration: Incorporating carbon capture for environmental compliance. *Engineering Science & Technology Journal, 5*(4), 1184–1202.

Orujov, A., Coddington, K., & Aryana, S. A. (2023). A review of CCUS in the context of foams, regulatory frameworks and monitoring. Energies, 16(7), 3284.

Osman, A. I., Chen, L., Yang, M., et al. (2022). Cost, environmental impact, and resilience of renewable energy under a changing climate: A review. *Environmental Chemistry Letters*, 1–24. https://doi.org/10.1007/S10311-022-01532-8

Osman, A. I., Deka, T. J., Baruah, D. C., & Rooney, D. W. (2023). Critical challenges in biohydrogen production processes from the organic feedstocks. *Biomass Conversion and Biorefinery,* 13, 8383–8401. https://doi.org/10.1007/s13399-021-01872-5

OurWorldinData. (2022). *Our World in Data*. https://ourworldindata.org/

Othmani, A., Magdouli, S., Kumar, P. S. K., Kapoor, A., Chellam, P. V., & Gökkuş, Ö. (2022). Agricultural waste materials for adsorptive removal of phenols, chromium (VI) and cadmium (II) from wastewater: A review. *Environmental Research, 204*. https://doi.org/10.1016/j.envres.2021.111984

P.R. Yaashikaa, Kumar, P. S., Saravanan, A., Karishma, S., & Rangasamy, G. (2023). A biotechnological roadmap for decarbonization systems combined into bioenergy production: Prelude of environmental life-cycle assessment. *Chemosphere, 329*, Article 138670. https://doi.org/10.1016/J.CHEMOSPHERE.2023.138670

Pwc. (2021). *Positioning Nigeria as Africa's leader in maize production for AfCFTA: Insights on global maize production and how Nigeria can position itself.* https://www.pwc.com/ng/en/assets/pdf/positioning-nigeria-as-africa-leader-in-maize-production-for-afcfta.pdf

Sandhu, K. S., Singh, N., & Malhi, N. S. (2007). Some properties of corn grains and their flours I: Physicochemical, functional and chapati-making properties of flours. *Food Chemistry, 101*, 938–946. https://doi.org/10.1016/j.foodchem.2006.02.040

Shah, S., Shah, M., Shah, A., & Shah, M. (2020). Evolution in the membrane-based materials and comprehensive review on carbon capture and storage in industries. *Emergent Materials, 3*(1), 33–44. https://doi.org/10.1007/s42247-020-00069-2

Shirzad, M., Karimi, M., & Abolghasemi, H. (2019). Polymer inclusion membranes with dinonylnaphthalene sulfonic acid as ion carrier for Co(II) transport from model solutions. *Desalination and Water Treatment, 144*, 185–200. https://doi.org/10.5004/dwt.2019.23575

Song, X., Wang, L., Gong, J., Zhan, X., & Zeng, Y. (2020). Exploring a new method to study the effects of surface functional groups on adsorption of CO_2 and CH_4 on activated carbons. *Langmuir, 36*, 3862–3870.

Soo, X. Y. D., Lee, J. J. C., Wu, W. Y., Tao, L., Wang, C., Zhu, Q., & Bu, J. (2024). Advancements in CO_2 capture by absorption and adsorption: A comprehensive review. *Journal of CO_2 Utilization, 81*, Article 102727. https://doi.org/10.1016/J.JCOU.2024.102727

Spigarelli, B. P., & Kawatra, S. K. (2013). Opportunities and challenges in carbon dioxide capture. *Journal of CO_2 Utilization, 1,* 69–87. https://doi.org/10.1016/j.jcou.2013.03.002

Stanger, R., Wall, T., Spörl, R., Paneru, M., Grathwohl, S., Weidmann, M., Scheffknecht, G., McDonald, D., Myöhänen, K., Ritvanen, J., et al. (2015). Oxyfuel combustion for CO_2 capture in power plants. International *Journal of Greenhouse Gas Control, 40,* 55–125. https://doi.org/10.1016/j.ijggc.2015.06.022

Storrs, K., Lyhne, I., & Drustrup, R. (2023). A comprehensive framework for feasibility of CCUS deployment: A meta-review of literature on factors impacting CCUS deployment. *International Journal of Greenhouse Gas Control*, *125*, 103878.

Theo, W. L., Lim, J. S., Hashim, H., Mustaffa, A. A., & Ho, W. S. (2016). Review of pre-combustion capture and ionic liquid in carbon capture and storage. *Applied Energy*, *183*, 1633–1663.

Toftegaard, M. B., Brix, J., Jensen, P. A., Glarborg, P., & Jensen, A. D. (2010). Oxy-fuel combustion of solid fuels. *Progress in Energy and Combustion Science, 36*(5), 581–625. https://doi.org/10.1016/j.pecs.2010.02.001

United Nations. (2022). What is climate change? https://www.un.org/en/climatechange/what-is-climate-change

Wang, C., Yang, G., Zhang, X., Shao, L., Lyu, G., Mao, J., Liu, S., & Xu, F. (2019). A kinetic study on the hydrolysis of corncob residues to levulinic acid in the $FeCl_3$–NaCl system. *Cellulose*, 26, 8313–8323.

Wilberforce, T., Baroutaji, A., Soudan, B., Al-Alami, A. H., & Olabi, A. G. (2019). *Outlook of carbon capture technology and challenges. Science of the Total Environment, 657,* 56–72. https://doi.org/10.1016/j.scitotenv.2018.11.424

Wohlthan, M., Thaler, B., Helf, A., Keller, F., Kaub, V., Span, R., Gräbner, M., & Pirker, G. (2024). Oxyfuel combustion based carbon capture onboard ships. *International Journal of Greenhouse Gas Control, 137*, 104234. https://doi.org/10.1016/j.ijggc.2024.104234

Wossen, T., Abdoulaye, T., Alene, A., Feleke, S., Menkir, A., & Manyong, V. (2017). Measuring the impacts of adaptation strategies to drought stress: The case of drought tolerant maize varieties. *Journal of Environmental Management, 203*, 106–113. https://doi.org/10.1016/j.jenvman.2017.06.058

Wu, F., Dellenback, P. A., & Fan, M. (2019). Highly efficient and stable calcium looping based pre-combustion CO_2 capture for high-purity H_2 production. Materials Today Energy, 13, 233–238.

Wu, F., Argyle, M. D., Dellenback, P. A., & Fan, M. (2018). Progress in O_2 separation for oxy-fuel combustion–A promising way for cost-effective CO_2 capture: A review. *Progress in Energy and Combustion Science, 67,* 188–205. https://doi.org/10.1016/j.pecs.2018.03.003

Yahaya-Shiru, M., Igwe, O., Onwuama, C. N., et al. (2023). Numerical geo-modelling of 'X-Field', central swamp II Depobelt, Niger Delta, Nigeria: Implications for carbon capture and sequestration. *International Journal of Environmental Science and Technology, 20,* 13673–13682. https://doi.org/10.1007/s13762-023-04885-x

Yang, C., Kim, Y., Bang, B., Jeong, S., Moon, J., Mun, T. Y., Jo, S., Lee, J., & Lee, U. (2020). Oxy-CFB combustion technology for use in power-generation applications. *Fuel, 267,* 117206. https://doi.org/10.1016/j.fuel.2020.117206

Yoro, K. O., & Daramola, M. O. (2020). CO_2 emission sources, greenhouse gases, and the global warming effect. In M. R. Rahimpour, M. Farsi, & M. A. Makarem (Eds.), *Advances in Carbon Capture* (pp. 3–28). Woodhead Publishing.

Yuan, Y., Wang, L., Zhuang, Y., Wu, Y., & Bi, X. (2024). Energy and economic assessment of oxy-fuel combustion CO_2 capture in coal-fired power plants. *Energies, 17*(10), 4626. https://doi.org/10.3390/en17104626

Zheng, W., Liu, X., Zhu, L., Huang, H., Wang, T., & Jiang, L. (2018). Pretreatment with γ-valerolactone/[Mmim]DMP and enzymatic hydrolysis on corncob and its application in immobilized butyric acid fermentation. *Journal of Agricultural and Food Chemistry*, *66*, 11709–11717.

Zou, X., Wang, Y., Tu, G., Zan, Z., & Wu, X. (2015). Adaptation and transcriptome analysis of *Aureobasidium pullulans*in corncob hydrolysate for increased inhibitor tolerance to malic acid production. *PLOS ONE*, *10*, e0121416.

APPENDIX

RESULTS FOR THE CARBON CAPTURE USING CORN COB EXPERIMENT

PARTICLE SIZE – 100 mics
BED HEIGHT - 5cm

FLOWRATE – 2L/min

Time(mins)	CO_2 Adsorbed Concentration(ppm)
5	632
10	578
15	520
20	486
25	433
30	422
35	417
40	435
45	423
50	411
55	409
60	403

PARTICLE SIZE - 250 mics

FLOWRATE – 2L/min

BED HEIGHT – 5cm

Time(mins)	CO_2 Adsorbed Concentration(ppm)
5	1341
10	1302
15	1258
20	1059
25	1031
30	899
35	869
40	609
45	575
50	555
55	670
60	697

PARTICLE SIZE – 500mics

BED HEIGHT – 5cm

FLOWRATE – 0.5L/min

Time(mins)	CO_2 Adsorbed Concentration(ppm)
5	452
10	418
15	400
20	405
25	566
30	538
35	508
40	471
45	433
50	402
55	404
60	403

PARTICLE SIZE – ABOVE 500mics

BED HEIGHT – 5cm

FLOWRATE – 0.5L/min

Time(mins)	CO_2 Adsorbed Concentration(ppm)
5	757
10	775
15	414
20	422
25	434
30	426
35	438
40	422
45	417
50	408
55	407
60	430

Packed Bed Adsorption of Carbon Dioxide

Laboratory column experiments were conducted isothermally in a 500 cm-long, 21 mm-diameter glass column at (29±2) ℃. A known mass of sample was filled to a height of 5.0 cm in the column at different particle sizes. Carbon dioxide and carbon monoxide from the CO_2 cylinder were connected from the bottom at a flow rate of 0.5 L/min. The concentration of carbon dioxide at the inlet was measured using a CO_2 detector, and the gas outlet from the fixed bed was periodically analyzed every 5 minutes for CO_2 concentration in parts per million (ppm). The flow rate was maintained at about 4,500 cm^3/min.

Time	Above 500 (A)	250-500 (B)	100-250 (C)	Less than 100 (D)
0	400	400	400	400
30	694	415	405	402
60	977	766	673	602
90	1241	1020	987	875
120	1245	1240	1024	1009
150	1250	1248	1243	1241

Time (minutes)	A	B	C	D
0	400	400	400	400
30	694	415	405	402
60	977	766	673	602
90	1241	1020	987	875
120	1245	1240	1024	1009
150	1250	1248	1243	1241

Time (minutes)	Ct/Co @ A	Ct/Co **@ B**	Ct/Co @ C	Ct/Co @ D
0	0.32	0.32	0.32	0.32
30	0.4552	0.332	0.324	0.3216
60	0.7816	0.5128	0.4384	0.3816
90	0.9928	0.916	0.7896	0.7
120	0.996	0.992	0.8992	0.8472
150	0.9984	0.9984	0.9944	0.9928

Note: A = >500µm, B = 250 – 500µm, C = 100 – 250µm, D = 100µm

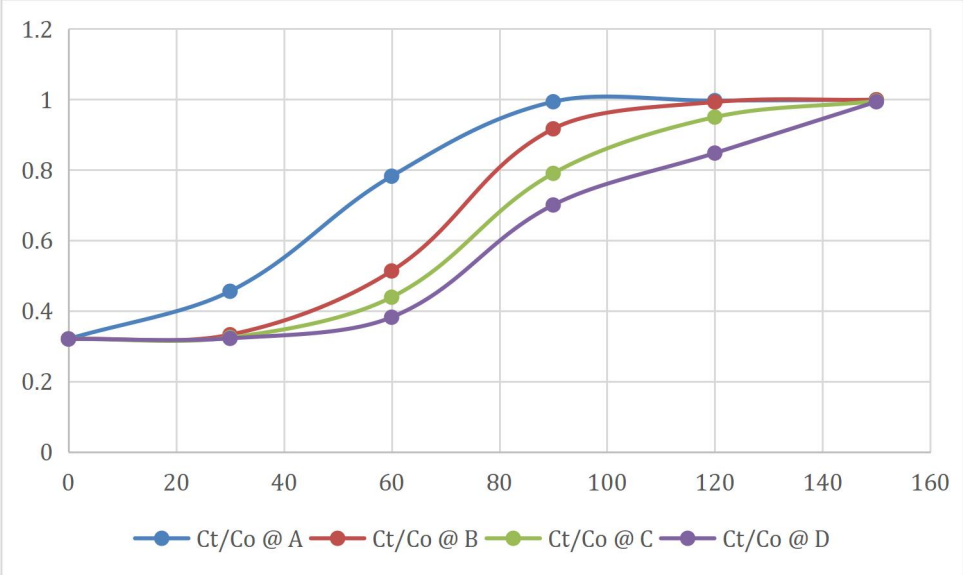

Figure 4.--: Breakthrough curve for sample

Parameter	**Value**
Breakpoint, $t_{u\,@}$ A	
Breakpoint, $t_{u\,@}$	

Breakpoint, $t_{u\,@}$ C	
Breakpoint, $t_{u\,@}$ D	
Dead point, $t_{t\,@}$ A	
Dead point, $t_{t\,@}$ B	
Dead point, $t_{t\,@}$ C	
Dead point, $t_{t\,@}$ D	
Total capacity to breakpoint, $\left({}^{t_u}/_{t_t}\right)_{@\,A}$	
Total capacity to breakpoint, $\left({}^{t_u}/_{t_t}\right)_{@\,B}$	
Total capacity to breakpoint, $\left({}^{t_u}/_{t_t}\right)_{@\,C}$	
Total capacity to breakpoint, $\left({}^{t_u}/_{t_t}\right)_{@\,D}$	
The length of the used bed, $H_B = \frac{tu}{t_t} H_{T\,@\,A}$	
The length of the used bed, $H_B = \frac{tu}{t_t} H_{T\,@\,B}$	
The length of the used bed, $H_B = \frac{tu}{t_t} H_{T\,@\,C}$	
The length of the used bed, $H_B = \frac{tu}{t_t} H_{T\,@\,D}$	
Total CO_2 adsorbed, $C_o \times Q \times t_t \times \rho_{@\,A}$	
Total CO_2 adsorbed, $C_o \times Q \times t_t \times \rho_{@\,B}$	
Total CO_2 adsorbed, $C_o \times Q \times t_t \times \rho_{@\,C}$	
Total CO_2 adsorbed, $C_o \times Q \times t_t \times \rho_{@\,D}$	

Note: Density of CO_2 = 0.00198g/cm^3

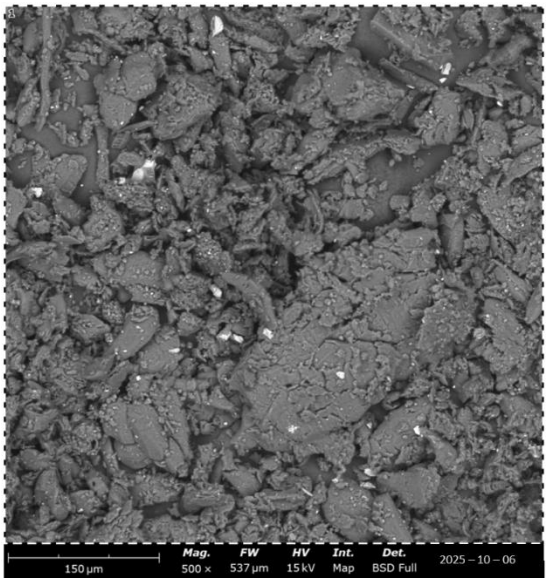

Element Number	Element Symbol	Element Name	Atomic Conc.	Weight Conc.
6	C	Carbon	90.05	76.31
20	Ca	Calcium	1.36	3.84
19	K	Potassium	1.38	3.80
30	Zn	Zinc	0.65	3.00
14	Si	Silicon	1.38	2.74
9	F	Fluorine	1.68	2.25
26	Fe	Iron	0.49	1.92
15	P	Phosphorus	0.87	1.90
13	Al	Aluminium	0.91	1.74
12	Mg	Magnesium	0.65	1.12
17	Cl	Chlorine	0.35	0.86
16	S	Sulfur	0.23	0.52
47	Ag	Silver	0.00	0.00
22	Ti	Titanium	0.00	0.00
11	Na	Sodium	0.00	0.00

FOV: 537 µm, Mode: 15kV - Map, Detector: BSD Full, Time: OCT 6 2025 16:47

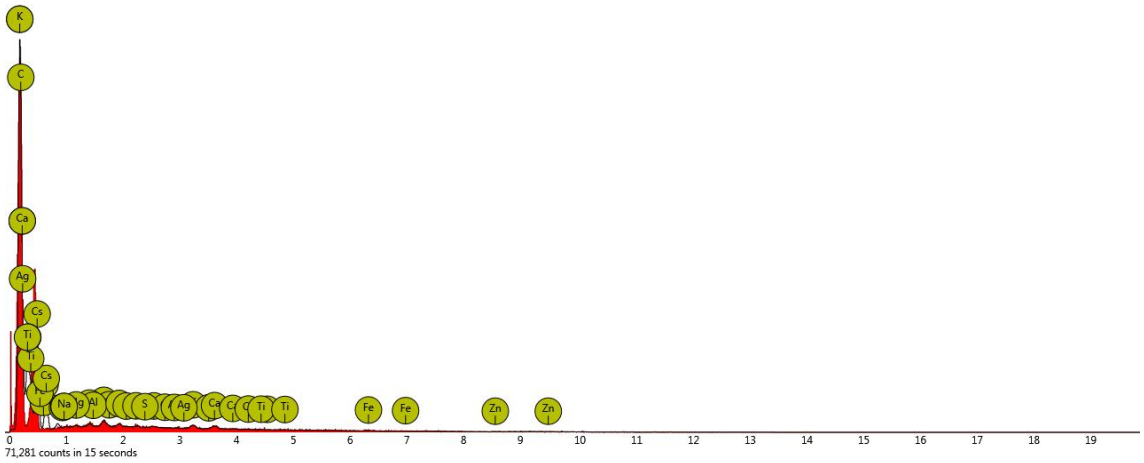

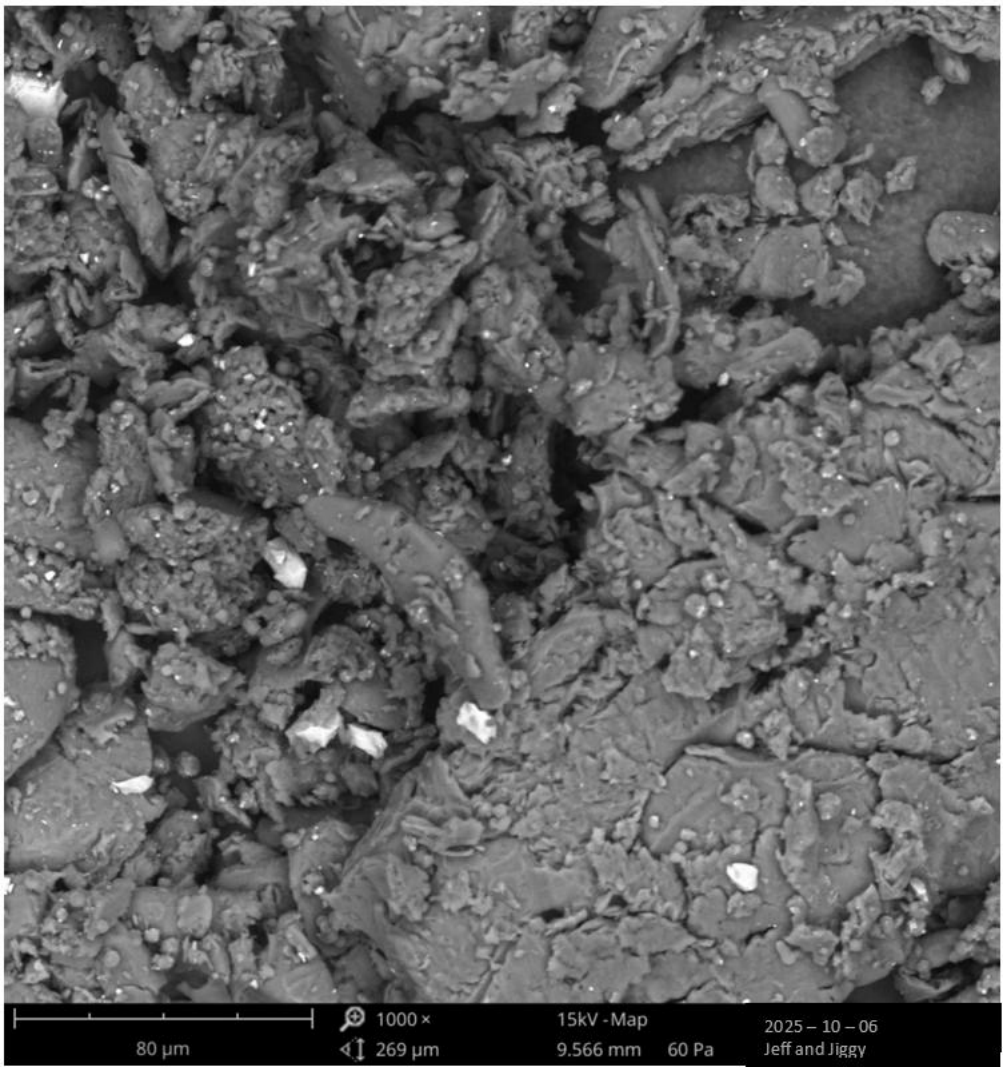
80 µm
1000 ×
269 µm
15kV - Map
9.566 mm
60 Pa
2025 – 10 – 06
Jeff and Jiggy

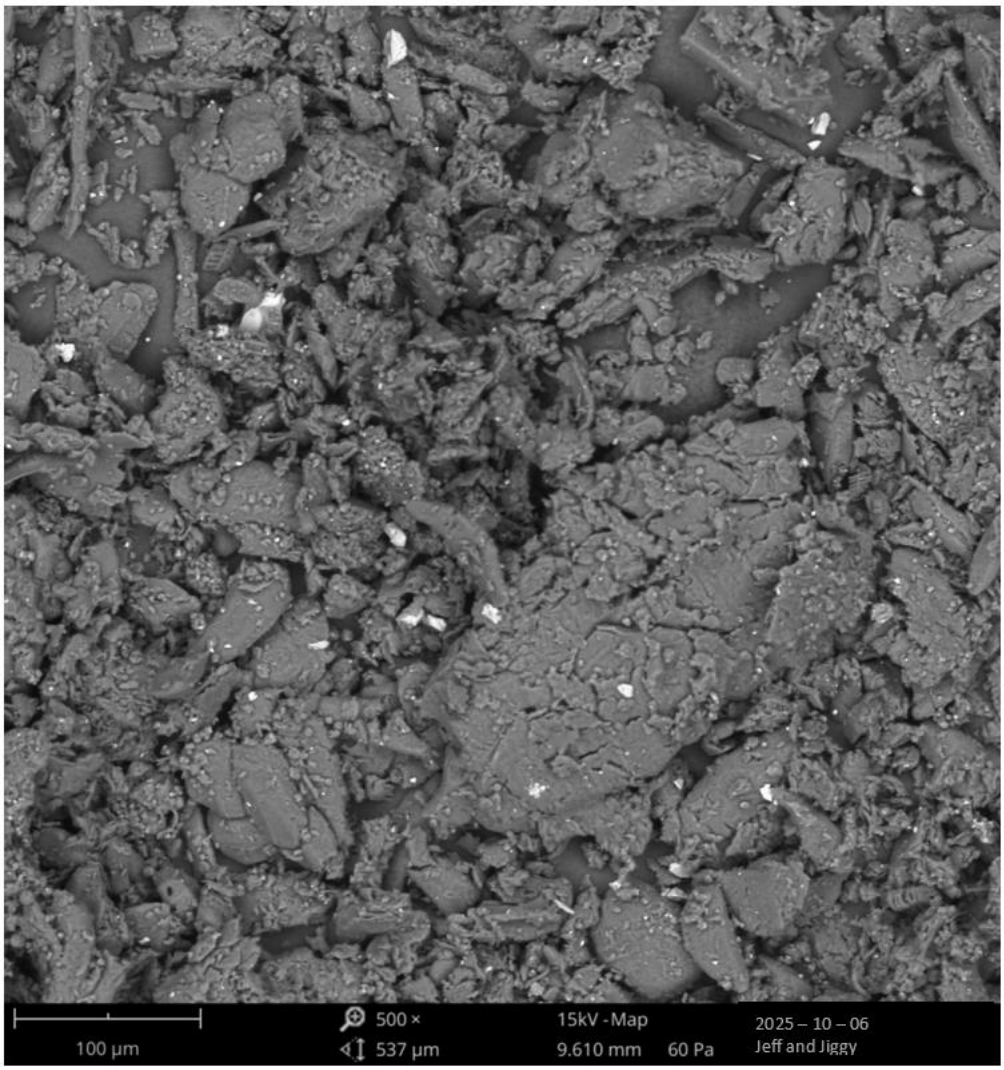
100 µm
500 ×
537 µm
15kV - Map
9.610 mm
60 Pa
2025 – 10 – 06
Jeff and Jiggy

Filename:	C\Username\Admins...Jeff-Jiggy
Operator ID:	Jeff-Jiggy
Sample Weight:	12.836mg
Comment:	TGA/DTA

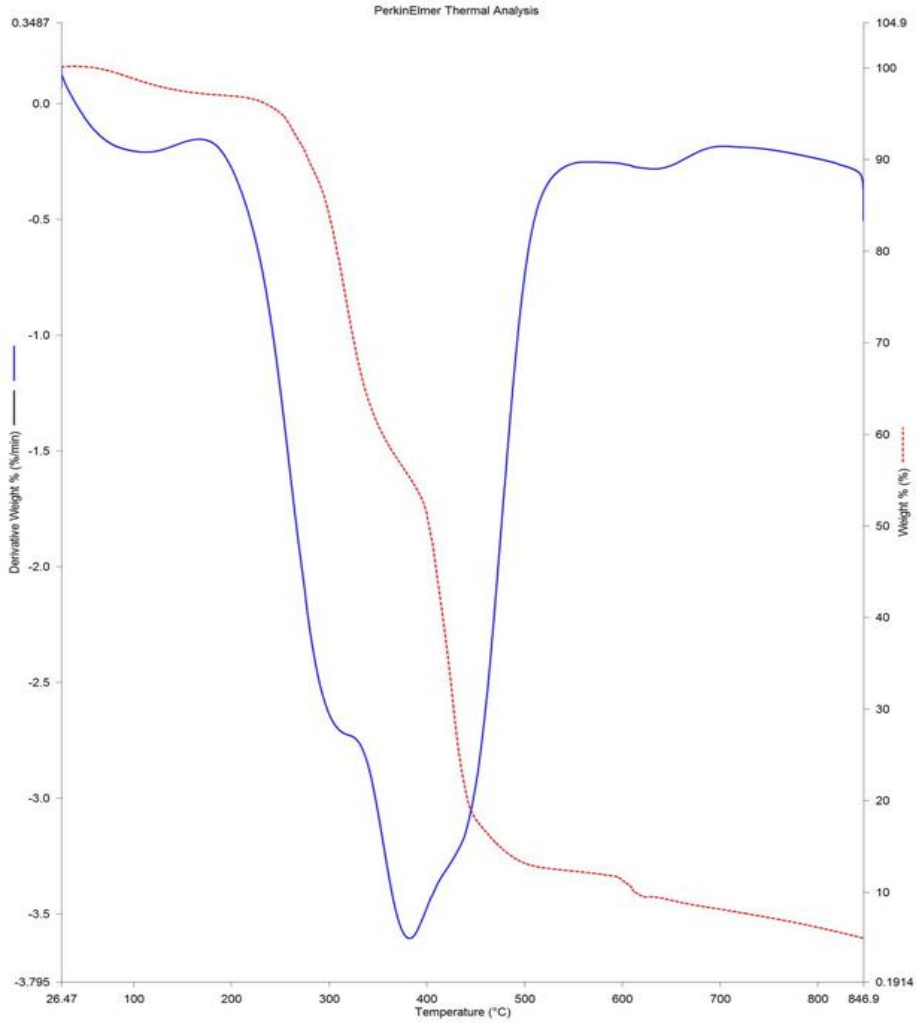

Filename:	C\Username\Admins...Jeff-Jiggy
Operator ID:	Jeff-Jiggy
Sample Weight:	12.836mg
Comment:	TGA/DTA

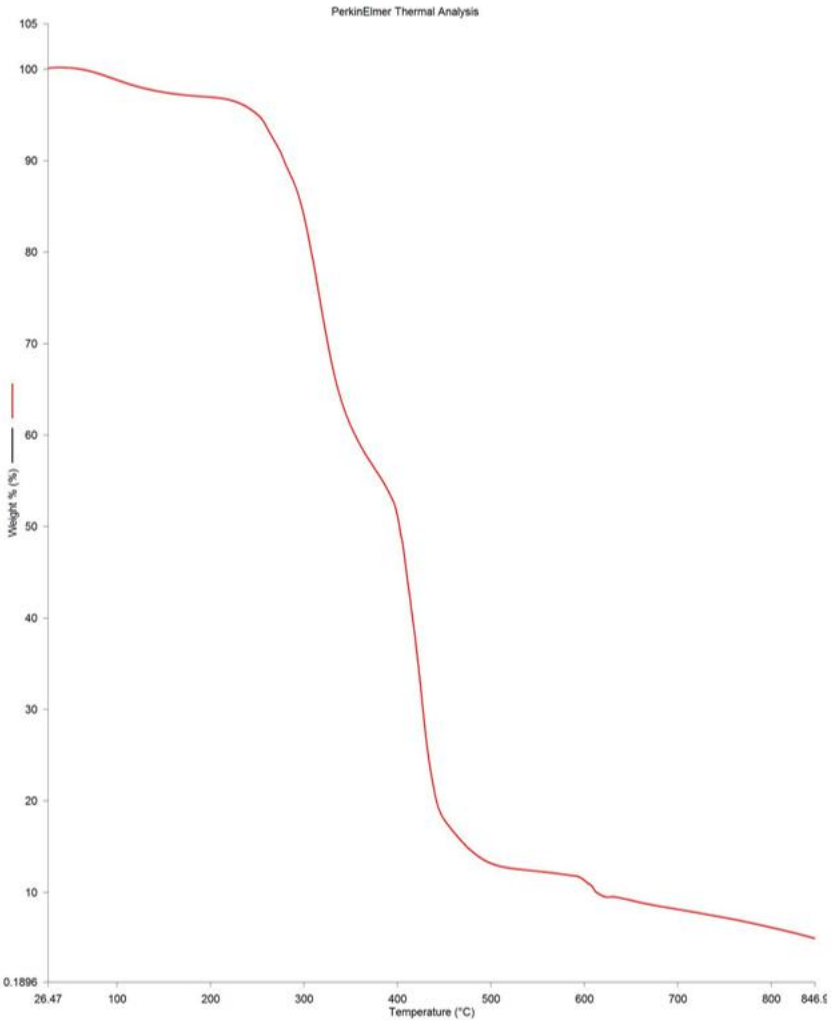

ADSORPTION EFFICIENCIES

$$Adsorption\ Efficiency\ = \frac{Initial\ CO_2 - Final\ CO_2}{Initial\ CO_2} \times 100\%$$

For 100 mics
Initial CO2 concentration = 632
Final CO2 concentration = 403

$$Adsorption\ Efficiency\ = \frac{632 - 403}{632} \times 100\%$$
$$Adsorption\ Efficiency\ = 36.234\%$$

For 250 mics
Initial CO2 concentration = 1341
Final CO2 concentration = 697

$$Adsorption\ Efficiency\ = \frac{1341 - 697}{1341} \times 100\%$$
$$Adsorption\ Efficiency\ = 48.024\%$$

For 500 mics
Initial CO2 concentration = 452
Final CO2 concentration = 403

$$Adsorption\ Efficiency\ = \frac{452 - 403}{452} \times 100\%$$
$$Adsorption\ Efficiency\ = 10.841\%$$

For Above 500 mics
Initial CO2 concentration = 757
Final CO2 concentration = 430

$$Adsorption\ Efficiency\ = \frac{757 - 430}{757} \times 100\%$$
$$Adsorption\ Efficiency\ = 43.197\%$$

ADSORPTION CAPACITIES

$$q_e = \frac{(C_O - C_e) \times V}{M}$$

V=Volume
M= Mass of Adsorbent
C_0 = 859 ppm (Initial CO_2 Concentration)
C_e = Final CO2 Concentration at Equilibrium

For 100 mics
Volume = 120L
C_0 = 859ppm
C_e = 403ppm
M = 18.62

$$q_e = \frac{(859 - 403) \times 120}{18.62}$$

$$q_e = 2939 \text{ppm·L/g}$$

For 250 mics
Volume = 120L
C_0 = 859ppm
C_e = 697ppm
M = 35.55

$$q_e = \frac{(859 - 697) \times 120}{35.55}$$

$$q_e = 547 \text{ppm·L/g}$$

For 500 mics
Volume = 30L
C_0 = 859ppm
C_e = 403ppm
M = 37.24

$$q_e = \frac{(859 - 403) \times 30}{37.24}$$

$$q_e = 367 \text{ppm·L/g}$$

For Above 500 mics
Volume = 30L
C_0 = 859ppm

C_e = 430ppm
M = 14.04

$$q_{e=}\frac{(859-430)\times 30}{14.04}$$

$$q_{e=916 ppm\cdot L/g}$$

KINETIC ANALYSIS

Experimental Data
PESUDO FIRST ORDER

Time(t)	**CO_2 Adsorbed Concentration (ppm)qt**	qe-qt	In(qe-qt)
5	632	0	-
10	578	54	3.9890
15	520	112	4.7185
20	486	146	4.9836
25	433	199	4.7791
30	422	210	5.3471
35	417	215	5.3706
40	435	197	5.2832
45	423	209	5.3423
50	411	221	5.3981
55	409	223	5.4072
60	403	229	5.4337

Particle Size: 100 mics, Flow Rate: 2 L/min, Bed Height: 5 cm

FOR 250mics

Time(t)	**CO_2 Adsorbed Concentration (ppm)qt**	qe-qt	In(qe-qt)
5	1341	0	—
10	1302	39	3.664
15	1258	83	4.419
20	1059	282	5.642
25	1031	310	5.737
30	899	442	6.091
35	869	427	6.158
40	609	732	6.598
45	575	766	6.640
50	555	786	6.668
55	670	671	6.509
60	697	644	6.469

Particle Size: 250 mics, Flow Rate: 2 L/min, Bed Height: 5 cm

FOR 500 mics:

Time(t)	**CO_2 Adsorbed Concentration (ppm)qt**	qe-qt	In(qe-qt)
5	452	114	4.7362
10	418	148	4.9972

15	400	166	5.1119
20	405	161	5.0814
25	566	0	—
30	538	28	3.3322
35	508	58	4.0604
40	471	95	4.5539
45	433	133	4.8903
50	402	164	5.0999
55	404	162	5.0876
60	403	163	5.0933

Particle Size: 500 mics, Flow Rate: 2 L/min, Bed Height: 5 cm

PSEUDO SCOND ORDER

Particle Size: 100 mics, Flow Rate: 2 L/min, Bed Height: 5 cm

Time(t)	**CO_2 Adsorbed Concentration (ppm)qt**	t/qt
5	632	0.0079
10	578	0.0173
15	520	0.0288
20	486	0.0411
25	433	0.0577
30	422	0.0711
35	417	0.0839
40	435	0.0920
45	423	0.1064
50	411	0.1217
55	409	0.1345

60	403	0.1489

Particle Size: 250 mics, Flow Rate: 2 L/min, Bed Height: 5 cm

Time(t)	**CO_2 Adsorbed Concentration (ppm)qt**	t/qt
5	1341	0.0037
10	1302	0.0077
15	1258	0.0119
20	1059	0.0189
25	1031	0.0242
30	899	0.0333
35	869	0.0403
40	609	0.0657
45	575	0.0783
50	555	0.0901
55	670	0.0821
60	697	0.0861

PSEUDO SCOND ORDER

Particle Size: 500 mics, Flow Rate: 2 L/min, Bed Height: 5 cm

Time(t)	**CO_2 Adsorbed Concentration (ppm)qt**	t/qt
5	452	0.0111
10	418	0.0239
15	400	0.0375
20	405	0.0494

25	566	0.0441
30	538	0.0558
35	508	0.0689
40	471	0.0849
45	433	0.1039
50	402	0.1244
55	404	0.1361
60	403	0.1489

Particle Size: >500 mics, Flow Rate: 2 L/min, Bed Height: 5 cm

Time(t)	**CO_2 Adsorbed Concentration (ppm)qt**	t/qt
5	757	0.0066
10	775	0.0129
15	414	0.0362
20	422	0.0474
25	434	0.0576
30	426	0.0704
35	438	0.0800
40	422	0.0948
45	417	0.1079
50	408	0.1225
55	407	0.1351
60	430	0.1395

ADSORPTION ISOTHERM

Langmuir experimental data

Ce	**Qe**	**Ce/Qe**
50	1500	0.0333
100	2800	0.0357

150	3200	0.0469
200	3500	0.0571
250	3700	0.0676
300	4000	0.0750
400	4300	0.0930
500	4500	0.1111
600	4600	0.1304
700	4650	0.1505

FREUNDLICH experimental data

Ce	**Qe**	**ln(Ce)**	**ln(Qe)**
50	1500	3.9120	7.3132
100	2800	4.6052	7.9374
150	3200	5.0106	8.0709
200	3500	5.2983	8.1605
250	3700	5.5215	8.2161
300	4000	5.7038	8.2940
400	4300	5.9915	8.3664
500	4500	6.2146	8.4118
600	4600	6.3969	8.4338
700	4650	6.5511	8.4446

Experimental Flow Chart